https://doi.org/10.5194/egusphere-2024-1498
Preprint. Discussion started: 23 May 2024

High-resolution analyses of concentrations and sizes of black carbon particles deposited on northwest Greenland over the past 350 years - Part 2: Seasonal and temporal trends in black carbon originated from fossil fuel combustion and biomass burning

Kumiko Goto-Azuma[1,2], Yoshimi Ogawa-Tsukagawa[1], Kaori Fukuda[1], Koji Fujita[3], Motohiro Hirabayashi[1], Remi Dallmayr[1,a], Jun Ogata[1], Nobuhiro Moteki[4], Tatsuhiro Mori[5], Sho Ohata[3], Yutaka Kondo[1], Makoto Koike[6], Sumito Matoba[7], and Teruo Aoki[1]

[1]National Institute of Polar Research, Tachikawa, Tokyo, 190-8518, Japan
[2]SOKENDAI, Shonan Village, Hayama, Kanagawa, 240-0193, Japan
[3]Nagoya University, Nagoya, 464-8601, Japan
[4]Tokyo Metropolitan University, Hachioji, Tokyo, 192-0397, Japan
[5]Keio University, Yokohama, Kanagawa, 223-8521, Japan
[6]University of Tokyo, Bunkyo-ku, Tokyo, 113-0033, Japan
[7]Hokkaido University, Sapporo, 060-0819, Japan
[a]Now at Alfred Wegener Institute for Polar and Marine Research, Bremerhaven, Germany

Correspondence to: Kumiko Goto-Azuma (kumiko@nipr.ac.jp)

Abstract. The roles and impacts of black carbon (BC), an important aerosol species affecting Earth's radiation budget, are not well understood owing to lack of accurate long-term observations. To study the temporal changes in BC since the pre-industrial period, we analysed BC in an ice core drilled in northwest Greenland. Using an improved technique for BC measurement and a continuous flow analysis system, we obtained accurate and high temporal resolution records of BC particle size and mass/number concentrations for the past 350 years. Number and mass concentrations, which both started to increase in the 1870s associated with inflow of anthropogenically derived BC, reached their maxima in the 1910s–1920s and then subsequently decreased. On the basis of backward trajectory analyses, we found that North America was the dominant source region of the anthropogenic BC in the ice core. The increase in anthropogenic BC shifted the annual concentration peaks of BC from summer to winter–early spring. After BC concentrations diminished to pre-industrial levels, the annual peak concentration of BC returned to the summer. We found that anthropogenic BC particles were larger than biomass burning BC particles. By separating the BC in winter and summer, we reconstructed the temporal variations in BC that originated from biomass burning, including the period with large anthropogenic input. The BC that originated from biomass burning showed no trend of increase until the early 2000s. Finally, possible albedo reductions due to BC are discussed. Our new data provide

https://doi.org/10.5194/egusphere-2024-1498
Preprint. Discussion started: 23 May 2024

key information for validating aerosol and climate models, thereby supporting improved projections of future climate and environment.

1 Introduction

Black carbon (BC) particles, which are emitted by incomplete combustion of biomass and fossil fuels, play important roles in Earth's radiation budget and thus in climate change (Bond et al., 2013; Moteki, 2023; Matsui et al., 2022; Legrand et al., 2016). In turn, changes in climate can affect emissions of BC from biomass burning through natural processes such as wildfires. Global warming is considered a major cause of the recent increase in large wildfires globally that can cause serious damage to ecosystems and human society (Calkin et al., 2023; Keeley and Syphard, 2021; Wang et al., 2021; Keane et al., 2008). Increased occurrence of large wildfires in the future could affect Earth's radiation budget, and change the frequency at which certain regions are exposed to serious hazard. Changes in fossil fuel combustion since the Industrial Revolution have changed Earth's radiation budget and contributed to the warming or cooling over the past century (Shindell and Faluvegi, 2009; McConnell et al., 2007; Breider et al., 2017). To understand the effects of BC on the radiation budget and of the impact of climate change on BC emissions, the long-term changes in the concentrations and size distributions of BC particles should be known. Data obtained since the pre-industrial period are particularly valuable because we cannot fully understand the anthropogenic effects without characterizing BC in a pristine environment. The Arctic is the key region for clearer elucidation of the roles of BC because the Arctic has warmed at a rate four times faster than that of the global average over the past half century, leading to drastic changes such as sea ice retreat, enhanced glacier mass loss, and ecosystem changes (Rantanen et al., 2022). Despite numerous studies based on observations and aerosol/climate models (e.g., Bond et al., 2013 and references therein), we have only limited knowledge on BC owing to lack of accurate long-term in situ observations (Mori et al., 2019). For the Arctic region, data are particularly sparse and few long-term records of BC size distribution exist.

Although there have been no direct observations before the past few decades, ice cores drilled in the Arctic have provided long-term records of BC. Development of the Single-Particle Soot Photometer (hereafter, SP2; Droplet Measurement Technologies, USA) (Stephens et al., 2003; Baumgardner et al., 2004) enabled measurements of BC in Arctic ice cores, where BC concentrations are low and sample volumes are limited (McConnell et al., 2007; Zdanowicz et al., 2018; Zennaro et al., 2014; Osmont et al., 2018). A continuous flow analysis (CFA) system is often used with the SP2 for high-resolution analysis of ice cores (McConnell et al., 2007; Zdanowicz et al., 2018; Zennaro et al., 2014). With an SP2 attached to a CFA system,

https://doi.org/10.5194/egusphere-2024-1498
Preprint. Discussion started: 23 May 2024

McConnell et al. (2007) reconstructed BC mass concentrations in central and southern Greenland since the pre-industrial period. They showed that BC concentration began a gradual rise after 1850, which was followed by rapid increase around 1890, a peak at around 1910, and then erratic decline through the late 1940s, followed by a sharp drop in the 1950s. They attributed the increase to BC derived mainly from fossil fuel combustion in North America. Similar anthropogenic temporal trends have been reported for other Greenland sites (McConnell, 2010). The BC flux records presented by McConnell (2010) suggest that the anthropogenically derived increase in BC was substantially less in northern Greenland than in southern Greenland, which is closer to the emission sources in North America and Western Europe. McConnell et al. (2007) also reported that the greatest increase in anthropogenic BC occurs in winter. However, no BC particle size data from Greenland ice cores have been published to date.

At Arctic sites outside Greenland, only a few ice cores have been analysed for BC. An ice core from Holtedahlfonna (Svalbard) indicated that BC mass concentration started to increase after 1850 and peaked around 1910, similar to the BC record of ice cores from Greenland (Ruppel et al., 2014). BC concentrations in the Holtedahlfonna core increased again between 1970 and 2004, reaching unprecedented values in the 1990s. This increase is not seen in Greenland ice cores, and contradicts atmospheric BC observations from Svalbard and other Arctic sites (Sharma et al., 2013), which indicate declining concentrations of atmospheric BC. Ruppel et al. (2014) attributed the differences partly to the different sources of anthropogenic BC affecting Svalbard and Greenland attributable to different air mass trajectories. They also suggested that changes in scavenging efficiency might have affected the Holtedahlfonna BC record. An ice core from Lomonosovfonna, another site in Svalbard (Osmont et al., 2018), showed gradual increase in BC during 1800–1859, followed by dramatic increase from 1860. The concentrations displayed two maxima at around 1870 and 1895, before they started to decline. Between 1910 and 1949, concentrations of BC were low. In contrast to the concentrations of BC in Greenland, another notable increase was evident in the Lomonosovfonna core after 1940, and the concentrations were at their highest in the 1950s and 1960s. The BC concentrations started to decrease in the 1970s, i.e., much later than the start of the decline in Greenland. The authors argued that the differences between Greenland and Lomonosovfonna are partly related to the different source regions of the air masses reaching Greenland and Svalbard.

The differences between the Holtedahlfonna and Lomonosovfonna records might also reflect different methods used for the measurement of BC mass concentration. The samples from the Holtedahlfonna ice core were filtered, and then the filters were analysed for BC using a thermal–optical method (Osmont et al., 2018), whereas the Lomonosovfonna and

https://doi.org/10.5194/egusphere-2024-1498
Preprint. Discussion started: 23 May 2024

Greenland ice cores were analysed using an SP2. Uncertainties regarding the filtering efficiency (Ruppel et al., 2014) and the effects of dust particles on the thermal–optical method could partly explain the differences in the long-term trends in BC concentrations. Furthermore, melt–freeze cycles that commonly occur at ice coring sites in Svalbard would have affected the BC concentrations (Osmont et al., 2018). Moreover, melt–freeze cycles could have agglomerated the BC particles to larger sizes beyond the detection range of a standard SP2 (Osmont et al., 2018; Wendl et al., 2014). An ice core BC record from the Devon Ice Cap in the Canadian Arctic was also found to differ from the records of Greenland ice cores (Zdanowicz et al., 2018). Although such differences could be partly attributable to different BC source regions, melt–freeze cycles could have also affected the Devon Ice Cap record. To investigate whether melt–freeze cycles did affect the derived BC concentrations, we need to know the sizes of the BC particles.

Even for ice cores drilled at sites where summer melting seldom occurs, such as those from interior Greenland, it is important to investigate the size distributions of BC particles to verify whether they are within the detection range of the SP2 instrument. This is because the sizes of BC particles in snow are often larger than those in the atmosphere (Schwarz et al., 2013; Mori et al., 2019) and exceed the detection range of a standard SP2, which is usually between approximately 70 and 850 nm (Mori et al., 2019). If a large proportion of BC particles have a diameter of >850 nm, the BC mass concentrations would be underestimated (Mori et al., 2019; Goto-Azuma et al., submitted). Furthermore, if an ultrasonic nebuliser, such as the U5000AT (CETAC Technologies, USA), was used with a standard SP2, as was the case in most previous studies of BC in ice cores (McConnell et al., 2007; Kaspari et al., 2011; Zennaro et al., 2014; Bisiaux et al., 2012a, b; Wang et al., 2015; Zdanowicz et al., 2018; Du et al., 2020), the upper limit of detectable BC size would have been <850 nm (Goto-Azuma et al, submitted). Because the nebulizing efficiency of this type of nebulizer varies markedly within this size range, variation in efficiency should be considered when calculating accurate mass concentrations and size distributions (Ohata et al., 2013). However, this was not taken into account in most previous ice core studies. It is therefore important to analyse Arctic ice cores using an instrumental set-up that allows detection of BC particles with diameter of >850 nm, and also to consider the size-dependent efficiency of the nebulizer. We developed a CFA system that includes a BC unit, which allows accurate high-resolution measurement of concentrations and size distributions of BC particles with diameter between 70 nm and 4 μm. Using this system, we analysed an ice core drilled at the SIGMA-D site in northwest Greenland. The details of this new system and its performance are described in the companion paper (Goto-Azuma et al., submitted). In this study, we analysed the data and investigated the

https://doi.org/10.5194/egusphere-2024-1498
Preprint. Discussion started: 23 May 2024

temporal variability in concentration and size distribution of BC that originated from fossil fuel combustion and biomass burning.

The BC detected in Arctic ice cores, together with NH_4^+ and specific organic materials (i.e., formate, levoglucosan, vanillic acid, and p-hydroxybenzoic acid), has been used to reconstruct past biomass burning (Ruppel et al., 2014; Zennaro et al., 2014; Grieman et al., 2017, 2018; Fischer et al., 2015; Pokhrel et al., 2020; Legrand et al., 2016). Although both BC and NH_4^+ have sources other than biomass burning (Osmont et al., 2018), levoglucosan, vanillic acid, and p-hydroxybenzoic acid primarily originate from biomass burning. However, the data regarding such organic materials usually have lower temporal resolution compared with that of BC and NH_4^+ data owing to limitations of the measurement techniques. Furthermore, little is known about their changes during atmospheric transport and post-depositional processes (Hennigan et al., 2010). Different ice core proxies often show different temporal and spatial trends in biomass burning activities (Legrand and de Angelis, 1996; Legrand and Mayewski, 1997; Legrand et al., 1992, 2016; Kawamura et al., 2012; Grieman et al., 2017, 2018; Rubino et al., 2016; Zennaro et al., 2014). Compared with the Global Charcoal Database, which has been used widely to investigate changes in biomass burning on centennial to orbital time scales (Power et al., 2010; Marlon et al., 2016), ice core proxy records usually have higher temporal resolution. Even monthly or seasonally resolved continuous records of BC and NH_4^+ for the past few centuries, millennia, and hundred thousand years have been derived from several Arctic ice cores, thereby allowing detection of high spikes in concentration in summer attributable to large boreal forest fires in northern North America and/or Siberia (Fischer et al., 2015; Zennaro et al., 2014). However, previous studies using BC as a biomass burning tracer have been restricted to the pre-industrial period. This is because BC originated from fossil fuel combustion contributed greatly to the total BC concentrations and obscured the temporal trends in BC related to biomass burning.

In this study, we reconstructed monthly resolved concentrations and sizes of BC particles in northwest Greenland over the past 350 years. The BC originated both from biomass burning and from fossil fuel combustion was distinguished owing to their different seasonal variability. In this paper, we discuss the temporal trends in the concentration and size of BC particles originated from both sources, and we investigate the BC source regions based on backward trajectory analyses. We then estimated the potential albedo reductions based on the monthly mean BC concentration data.

https://doi.org/10.5194/egusphere-2024-1498
Preprint. Discussion started: 23 May 2024

2 Materials and Methods

2.1 Ice core processing, analyses, and dating

A 222.7 m ice core was drilled at the SIGMA-D site (77.636° N, 59.120° W; 2100 m a.s.l.; Fig. 1) in northwest Greenland in spring 2014 (Matoba et al., 2015). The annual mean air temperature and accumulation rate at the site were estimated to be −25.6 °C and 0.23 w eq·yr^{-1}, respectively (Nagatsuka et al., 2021). The details of the ice core processing and analyses are described in the companion paper (Goto-Azuma et al., submitted to Atmospheric Chemistry and Physics); therefore, we provide only a brief summary here. The top 175.77 m of the core was divided into two vertical sections (Sections A and B) in the field. Section A was kept frozen and transported to the National Institute of Polar Research (NIPR) in Japan; Section B was cut, melted, and bottled in the field.

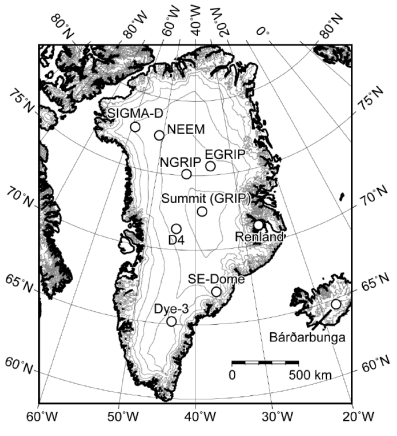

Figure 1: Location of the SIGMA-D site and that of other drill sites.

Down to the depth of 112.8 m in Section A, we cut quadrangular prism samples with a cross section of 34 mm × 34 mm. For the depth interval between 6.1 and 112.8 m, we analysed BC, stable water isotopes, and six elements (i.e., ^{23}Na, ^{24}Mg, ^{27}Al, ^{39}K, ^{40}Ca, and ^{56}Fe) using the NIPR CFA system. The top 6.1 m of Section A was too fragile to be analysed using the CFA system; hence, we manually cut it into segments of approximately 0.1 m. These “discrete samples” were decontaminated in a −20 °C cold room using a precleaned ceramic knife and then placed in powder-free plastic bags. They were then melted and transferred to precleaned glass and polypropylene bottles in a class 10,000 clean room. The samples in glass bottles were analysed for stable isotopes of water and BC. For the discrete samples, stable isotopes of water were analysed using a near-

https://doi.org/10.5194/egusphere-2024-1498
Preprint. Discussion started: 23 May 2024

infrared cavity ring-down spectrometer (L2120-i, Picarro Inc., USA), a high-precision vaporizer (A0211, Picarro Inc., USA), and an autosampler (PAL HTC9 - xt - LEAP, LEAP Technologies, USA). The precision of determination was ±0:05‰ for $\delta^{18}O$. The samples in the polypropylene bottles were analysed for six elements (i.e., ^{23}Na, ^{24}Mg, ^{27}Al, ^{39}K, ^{40}Ca, and ^{56}Fe) using an inductively coupled plasma mass spectrometer (7700 ICP-MS, Agilent Technologies, USA) in a class 10,000 clean room at NIPR.

Both the CFA samples and the discrete samples were analysed for BC using a Wide-Range SP2 (Mori et al., 2016), which is a modified version of the SP2 (Droplet Measurement Technologies, USA), and a concentric pneumatic nebulizer (Marin-5, Teldyne CETAC, USA). The combination of the Wide-Range SP2 and the pneumatic nebulizer enabled us to extend the range of the size of BC particles analysed (70 nm < diameter < 4 μm) to beyond that of the standard SP2 (70 nm < diameter < 600–850 nm). This combination and a careful calibration procedure enabled us to measure not only the concentration but also the diameter of BC particles. The analytical errors of the BC mass and number concentrations were estimated to be <16% (Mori et al., 2016). The reproducibility of the BC number and mass concentrations for repeated measurements was usually better than 10% (Mori et al., 2019). The detection limits of the BC number and mass concentrations were approximately 10 counts·L^{-1} and 0.01 μg·L^{-1}, respectively.

Depths of Section B above 61.2 m were analysed for Na^+, K^+, Mg^{2+} and Ca^{2+}, Cl^-, NO_3^-, and SO_4^{2-} using two ion chromatographs (ICS-2100, Thermo Fisher Scientific, USA) at Hokkaido University (Japan), whereas depths between 61.2 and 112.87 m were analysed for NH_4^+, Na^+, K^+, Mg^{2+}, Ca^{2+}, Cl^-, NO_3^-, and SO_4^{2-} using two ion chromatographs (ICS-2000, Thermo Fisher Scientific, USA) at NIPR. The limit of detection of Na^+ measured at Hokkaido University was 1 μg L^{-1}, whereas that measured at NIPR was 0.2 μg L^{-1}. Stable water isotopes were analysed for all samples from Section B using a near-infrared cavity ring-down spectrometer (L2130-i, Picarro, USA) and a high-throughput vaporizer (A0212, Picarro, USA) at Hokkaido University. The precision of determination was ±0:08‰ for $\delta^{18}O$. For dating purposes, tritium concentrations were measured using a liquid scintillation counter (LSC-LB3; Aloka Co. Ltd., Japan) at 0.05 m intervals for the depth interval 19.15–26.47 m (Nagatsuka et al., 2021).

Figure 2 shows the seasonal variability in Na and Na^+ concentrations, together with that in $\delta^{18}O$ (Goto-Azuma et al., submitted). Concentrations of Na and Na^+ show maxima in winter and minima in summer, whereas the $\delta^{18}O$ shows maxima in summer and minima in winter (Nagatsuka et al., 2021; Legrand and Mayewski, 1997; Mosher et al., 1993). As reported in the companion paper (Goto-Azuma et al., submitted), we dated Section B of the SIGMA-D core by annual layer counting

https://doi.org/10.5194/egusphere-2024-1498
Preprint. Discussion started: 23 May 2024

using mainly Na^+ (Nagatsuka et al., 2021). We supplementarily used Ca and $\delta^{18}O$ data when annual peaks of Na^+ were not clearly observed. Additionally, we used a tritium peak and volcanic SO_4^{2-} peaks as reference horizons (Nagatsuka et al., 2021). Because the CFA data from Section B and the discrete data from Section A agreed well (Fig. 2), we adopted the chronology of Section B for that of Section A. However, for the years before 1783, we made minor adjustments where high SO_4^{2-} peaks did not match the volcanic eruptions reported from study of other Greenland ice cores (Sigl et al., 2013). The uncertainties of dating were estimated to be less than ±2 years. The CFA data covered 1653–2002 (Goto-Azuma et al., submitted), and the data from the top 6.1 m covered the period 2003–2013. We divided one year into 12 months based on the assumption that the annual maxima and minima of Na^+ concentration correspond to 1 January and 1 July, respectively (Fig. 2). Each depth interval corresponding to a half year was evenly divided into six months. Using the CFA data, we calculated the annual mean and the monthly mean values of the number and mass concentrations of BC particles.

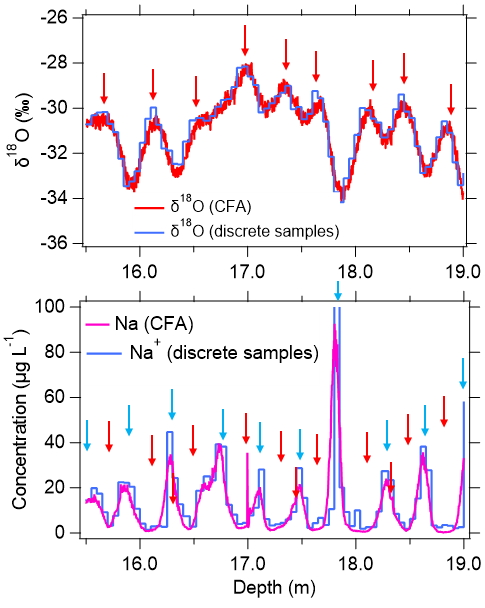

Figure 2: Concentrations of (a) $\delta^{18}O$ and (b) Na (and Na^+) (Goto-Azuma et al., submitted). Red and blue curves represent data obtained from CFA measurements and discrete sample measurements of the SIGMA-D core, respectively. Blue and red arrows indicate winter and summer, respectively. Winter and summer peaks were assumed to represent January 1 and July 1 of each year, respectively.

https://doi.org/10.5194/egusphere-2024-1498
Preprint. Discussion started: 23 May 2024

189

190 **2.2 Backward trajectory analysis**

191 To estimate the contributions of different air masses affecting the SIGMA-D and D4 sites (Fig. 1), we performed 10-day
192 backward trajectory analyses for the period 1958–2015. Dividing the globe into 21 regions (Fig. A1), we calculated the
193 contribution from each region. We used the Single-Particle Lagrangian Integrated Trajectory (HySPLIT) model developed by
194 the National Oceanographic and Atmospheric Administration (NOAA) (Stein et al., 2015). The initial air mass was set at three
195 elevations at each site (i.e., 500, 1000, and 1500 m above ground level), and the accumulated probability of the air mass in
196 each 1° grid cell was calculated. Assuming wet deposition of BC at the ice core sites, the air mass probability was weighted
197 with the local daily precipitation, i.e., if no precipitation occurred, the air mass was not considered, and vice versa. We used
198 ERA5 precipitation data produced by the European Centre for Medium-Range Weather Forecasts (Hersbach et al., 2020).
199 Details of the procedures are described in previous studies (Parvin et al., 2019; Nagatsuka et al., 2021; Nagatsuka et al., 2023).

200

201 **3 Results and Discussion**

202 **3.1 Impacts of anthropogenic emissions on long-term trends in concentrations and sizes of BC particles**

203 Figure 3 displays annual and decadal averages of number and mass concentrations of BC during the past 350 years. Notably,
204 monthly mean values could have been affected by the values of the adjacent few months, considering the resolution of the

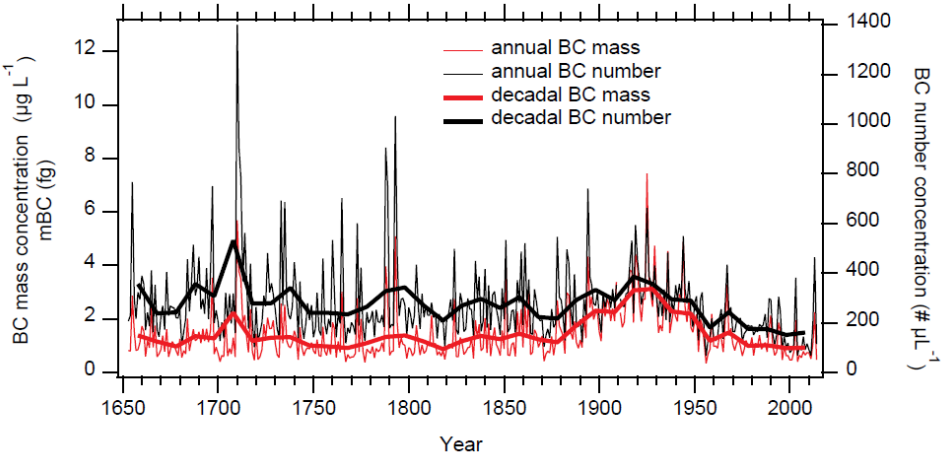

Figure 3: Annual mean (thin curves) and decadal mean (thick curves) concentrations of BC. Red and black curves represent mass and number concentrations, respectively.

https://doi.org/10.5194/egusphere-2024-1498
Preprint. Discussion started: 23 May 2024

CFA data (10–40 mm) estimated from signal dispersion tests (Goto-Azuma et al., submitted). Because we melted the core from the bottom to the top, the data for a few months after large BC concentration peaks could have been affected. However, the annual and decadal averages were unaffected by the CFA signal dispersion. Apart from sporadic sharp peaks in number and mass concentrations, their background levels started to increase in the 1870s, reached their maxima in the 1910s–1920s, and decreased again after the 1930s. In the 1960s, BC number and mass concentrations returned to their pre-industrial levels. In the 1980s and 1990s, number concentrations were below the pre-industrial level, whereas mass concentrations were similar to those of the pre-industrial level. Before 1850, the major sources of BC in Greenland were likely to have been biomass burning emissions from boreal forest fires (Legrand et al., 2016; McConnell et al., 2007; Zennaro et al., 2014). The increases in BC concentrations that occurred in the late 19th century to mid-20th century are likely attributable to inflow to Greenland of BC of anthropogenic origin, as reported previously (McConnell, 2010; McConnell et al., 2007).

Direct comparison between the BC concentrations in the SIGMA-D core and those in other Greenland ice cores is not strictly feasible owing to methodological differences. BC measurements in other Greenland ice cores were conducted using the standard SP2 coupled with an ultrasonic nebulizer (McConnell et al., 2007; McConnell, 2010; Zennaro et al., 2014). This setup allows for the measurement of BC particles with diameter of less than 600–650 nm (Goto-Azuma et al., submitted). In contrast, the measurements of the SIGMA-D ice core could detect BC particles with diameter up to 4 μm. Therefore, BC concentrations in other Greenland ice cores might have been underestimated during periods when the diameter of large proportions of BC particles exceeded approximately 650 nm. Owing to lack of information on size distributions, the extent of the underestimation for other Greenland ice cores remains unknown. As described in the companion paper (Goto-Azuma et al., submitted), if the measurement method used in the previous studies had also been used for the SIGMA-D ice core, the extent of underestimation would have depended on depth and hence on age. However, the general temporal trends in annual mean BC concentrations at the SIGMA-D site did not change notably if BC particles with diameter of >650 nm were excluded (Fig. 4). Therefore, it is informative to compare the BC concentration trends at the SIGMA-D site with those of other Greenland sites.

https://doi.org/10.5194/egusphere-2024-1498
Preprint. Discussion started: 23 May 2024

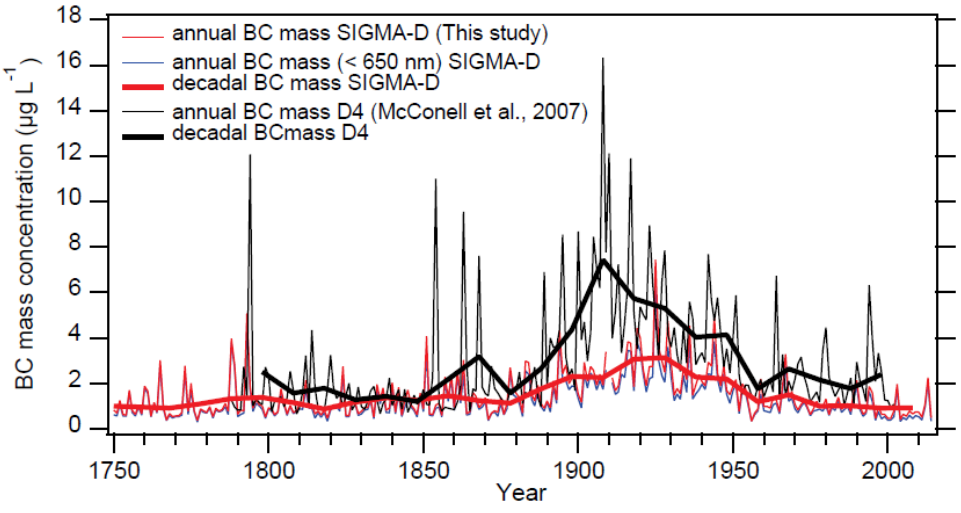

Figure 4: Annual mean (thin curves) and decadal mean (thick curves) mass concentrations of BC. Red and black curves represent BC concentrations at the SIGMA-D and D4 sites, respectively. Blue curves show annual BC concentrations for BC particles with diameter of <650 nm.

The long-term trends in BC mass concentrations at the SIGMA-D site are broadly similar to those at other ice core sites in Greenland (McConnell et al., 2007; McConnel., 2010), including the D4 site. However, the SIGMA-D core shows much lower anthropogenic BC concentrations, a later peak period, and later onset of the reductions in comparison with those of the D4 core (Fig. 4). This is in accord with the studies by McConnel et al. (2007) and McConnel (2010), which indicate that more southerly sites generally show higher anthropogenic BC concentrations, an earlier peak period, and earlier onset of the decline in anthropogenic BC concentrations in comparison with those of more northerly sites. The BC emission inventories for potential BC source regions indicate that emissions of anthropogenically derived BC started earlier in Europe than in North America, and that the decline in anthropogenic BC concentrations started earlier in North America than in Europe or the former USSR (Osmont et al., 2018). The emission inventories used by Osmont et al. (2018) were those adopted for the Coupled Model Intercomparison Project phase 5 (CMIP 5; Bauer et al., 2013; Eckhardt et al., 2023; Lamarque et al., 2010). If those emission inventories are reliable, then the slight difference in the temporal trends of BC concentrations would indicate that southern Greenland sites (e.g., the D4 site) had been influenced mainly by anthropogenic emissions from North America, whereas

https://doi.org/10.5194/egusphere-2024-1498
Preprint. Discussion started: 23 May 2024

242 northern Greenland sites (e.g., the SIGMA-D site) had been influenced by anthropogenic emissions from Europe and the
243 former USSR (in addition to those from North America), as was the case for anthropogenic sulphate (Goto-Azuma and Koerner,
244 2001). However, the results of our backward trajectory study do not support this hypothesis, as discussed below.

245 The 10-day backward trajectories for the SIGMA-D and D4 sites showed no contributions of air masses from
246 Antarctica (AT), Australia and New Zealand (AUS), South America (SAM), Southeast Asia (SEA), South Asia (SA), the
247 Antarctic Ocean (ATO), South Pacific Ocean (SPO), Indian Ocean (INO), and South Atlantic Ocean (SAO). The four regions
248 of the Middle East (ME), Africa (AF), East Asia (EA), and Central Asia (CA) showed maximum contributions of <0.05%. In
249 further analyses, we omitted the above 13 regions and focused on the eight regions of Europe (EU), the Greenland Ice sheet
250 (GrIS), Russia (RUS), North America (NA), the North Pacific Ocean (NPO), North Atlantic Ocean (NAO), Arctic Ocean (AO),
251 and Iceland (IC) (Fig. 5). Of these, GrIS, AO, NA, and NAO were found to be the major sources of the air masses arriving at
252 both the SIGMA-D site and the D4 site, although only NA represents a source of anthropogenic BC emissions. Therefore, the
253 temporal trends in anthropogenic BC at both SIGMA-D and D4 appear to reflect the trend of BC emission in NA.

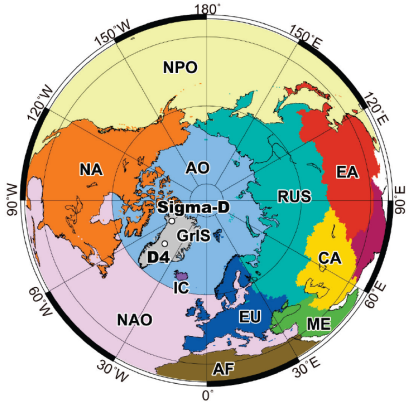

Figure 5: The 12 regions used for backward trajectory analyses (GrIS: Greenland Ice Sheet, NA: North America, EU: Europe, RUS: Russia, CA: Central Asia, EA: East Asia, ME: Middle East, AF: Africa, NPO: North Pacific Ocean, NAO: North Atlantic Ocean, AO: Arctic Ocean, and IC: Iceland).

254 The contributions of air masses from EU and RUS, which are regions with high levels of emission of anthropogenic
255 BC (Hoesly et al., 2018), were less than 4% and 1%, respectively, at both the SIGMA-D site and the D4 site, even in winter
256 when their contributions are at their maxima. To investigate the influence of contributions from EU and RUS in more detail,
257 we recalculated the air mass contributions by excluding GrIS and the oceanic regions of NPO, NAO, and AO where there are

https://doi.org/10.5194/egusphere-2024-1498
Preprint. Discussion started: 23 May 2024

no sources of BC emission. Although GrIS had the largest air mass contributions throughout the year and throughout the 10 days, we excluded it because most of the region is covered with ice and has very minor BC sources. The temporal variations in the contributions from NA, EU, RUS, and IC are plotted in Fig. 6, and the probability distributions of the air masses for the SIGMA-D and D4 sites are displayed in Fig. 7. In winter, when the anthropogenic input of BC is greatest at both the SIGMA-D site (see Sect 3.2) and the D4 site (McConnell et al., 2007), contributions from NA are the highest at both sites. At both sites, the contributions from EU and RUS increase in winter (Figs. 6 and 7) when air masses from distant sources can more easily reach the Arctic (Jurányi et al., 2023). Against our expectation based on CMIP 5 emission inventories, the contributions from EU were slightly greater at D4 than at SIGMA-D. The contributions from RUS were similar at both sites and comprised approximately 20% of the total at most. Although backward trajectory analyses showed that contributions from EU were slightly different between the SIGMA-D and D4 sites, the results suggested the opposite conclusion to that of an assumption based on the regional difference in emission inventories to explain the slight differences in the temporal trend of BC at the two sites.

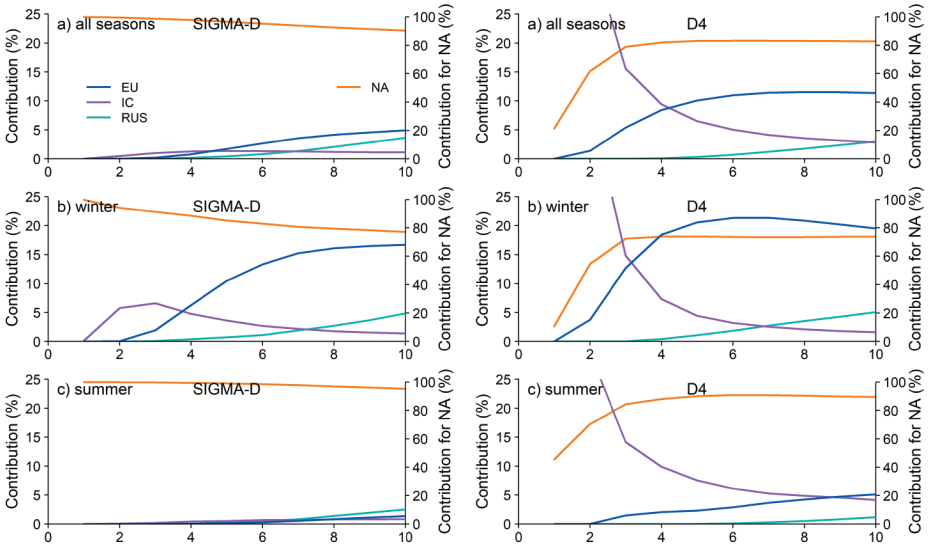

Figure 6: Temporal variability in contributions of air masses arriving at (left) the SIGMA-D site and (right) the D4 site from four regions: (a) averages of 12 months, (b) averages of winter months (December–February), and (c) averages of summer months (May–July). Right-hand axes indicate contributions from NA, left-hand axes indicate contributions from the other regions.

https://doi.org/10.5194/egusphere-2024-1498
Preprint. Discussion started: 23 May 2024

270

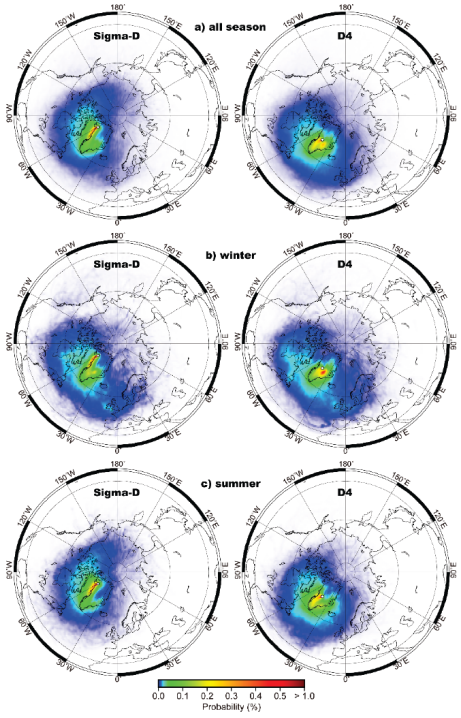

Figure 7: Probability distributions of air masses at (left) the SIGMA-D site and (right) the D4 site: (a) averages of all seasons, (b) averages of winter months (December–February), and (c) averages of summer months (May–July).

271 Notably, there are large uncertainties in emission inventories. Although the CMIP 5 emission inventories appear to
272 reproduce the temporal patterns in concentrations and fluxes of BC in Arctic ice cores better than those produced using the
273 Coupled Model Intercomparison Project phase 6 (CMIP 6) inventories, the reproduction of the magnitudes of the
274 concentrations and fluxes is better when using the CMIP 6 inventories (Eckhardt et al., 2023). A model intercomparison study,
275 which compared the modelling results obtained from 11 Earth System Models using CMIP 6 emission inventories with BC
276 records from ice cores (Moseid et al., 2022), revealed errors in European emission inventories. However, the study also showed
277 that BC concentrations in Northern Greenland ice cores reflected European emissions, contradicting our backward trajectory
278 analyses. It should be also noted that backward trajectory analyses are unable to capture the contributions of air masses
279 transported through the upper troposphere (Nagatsuka et al., 2021), which could be important when estimating the
280 contributions from distant sources. Currently, we are unable to explain the slightly different temporal trends in the BC records

https://doi.org/10.5194/egusphere-2024-1498
Preprint. Discussion started: 23 May 2024

281 from different ice cores in Greenland. Further elucidation of this topic will require additional modelling studies constrained by
282 accurate BC records from Greenland ice cores.

283 Figure 8 displays decadal mean mass and number size distributions of BC for different periods with different
284 anthropogenic inputs. We assumed that the mass size distribution follows a Gaussian distribution and thus we estimated the
285 mass median diameter (MMD), which is one of the measures of a BC size distribution. The decadal mean MMD was 226 nm
286 in the pre-industrial period of 1783–1792. It increased to 325 nm in the peak anthropogenic period of 1913–1922, and
287 subsequently decreased to 302 nm in 1993–2002 and 278 nm in 2003–2012. Number size distributions did not show noticeable
288 temporal change. To investigate the temporal changes in BC size distribution, we used the average mass of BC particles (mBC)
289 in addition to the MMD. The parameter mBC can be calculated by dividing the mass concentration by the number concentration.
290 Figure 9 shows the annual and decadal mean mBC and decadal mean MMD, together with the annual and decadal mean BC
291 mass concentrations. Of the two size parameters, mBC is easier to calculate than MMD; hence, it can be used to investigate
292 changes with high temporal resolution. Both the annual mean mBC and the decadal mean MMD started to increase in the
293 1830s and peaked in the 1910s–1920s, when the mass and number concentrations of BC were at their maxima. The peak values

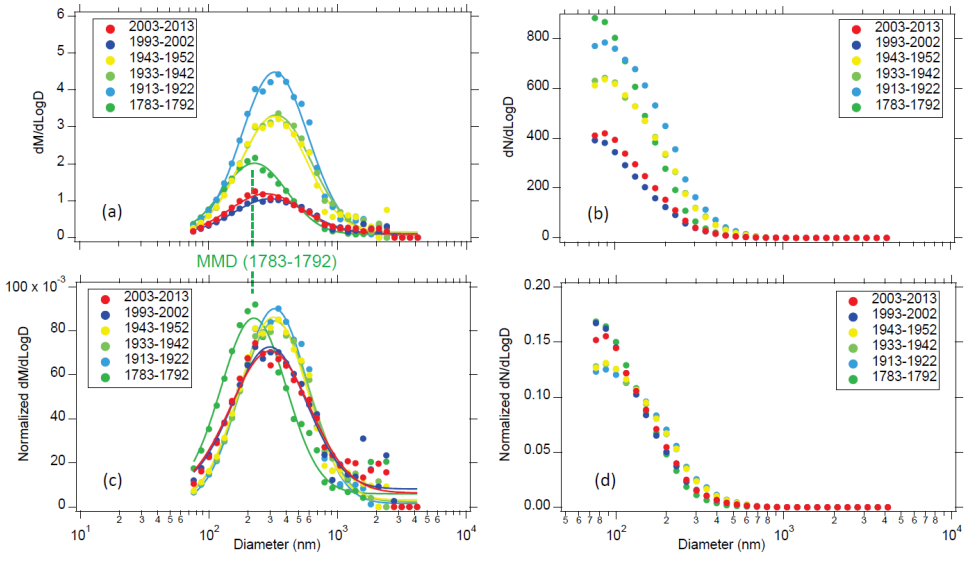

Figure 8: Temporal changes in decadal mean size distributions of BC particles: (a) and (b) non-normalized mass and number size distributions, respectively, and (c) and (d) normalized mass and number size distributions, respectively. Dotted line in (a) indicates the mass median diameter (MMD) for the period 1783–1792.

https://doi.org/10.5194/egusphere-2024-1498
Preprint. Discussion started: 23 May 2024

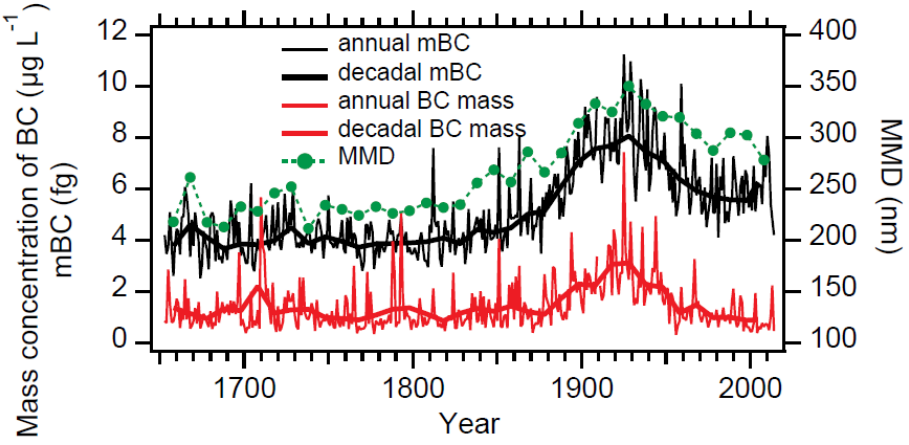

Figure 9: Annual and decadal mean mBC (black) and decadal mean MMD (green), together with annual and decadal mean BC mass concentration (red). Thin and thick solid lines denote annual and decadal means, respectively.

294 of MMD and mBC were approximately twice and 1.5 times, as high as the corresponding pre-industrial values, respectively.
295 Anthropogenically derived BC particles that arrived in northwest Greenland appear to have been larger than BC particles of
296 biomass burning origin. This is contrary to our expectation because it has been reported that the sizes of BC particles from
297 biomass burning are larger than those from anthropogenic emissions near the sources (Bond et al., 2013). In the 1920s or 1930s,
298 MMD and mBC both started to decrease, as did the mass and number concentrations of BC particles. However, in contrast to
299 BC concentrations, neither MMD nor mBC returned to their pre-industrial levels; instead, they remained approximately 1.3
300 and 1.5 times higher than their pre-industrial levels, respectively. We also notice that the start of the increases in mBC and
301 MMD appear to have occurred earlier than the increases in mass and number concentrations of BC by 30–40 years.
302
303 **3.2 Temporal changes in seasonal variations in concentrations and sizes of BC particles**
304 Figure 10 compares the monthly mean BC mass concentrations in three periods: the pre-industrial period, the period with high
305 anthropogenic input, and recent years when concentrations decreased and returned to pre-industrial levels. Changes are evident
306 in the seasonality of BC concentrations with respect to Na concentrations, which peak in winter. As reported by McConnell et
307 al. (2007) in relation to the D4 core, BC concentrations peaked in summer in the pre-industrial period, whereas they peaked in

https://doi.org/10.5194/egusphere-2024-1498
Preprint. Discussion started: 23 May 2024

308 late-winter to early spring during the peak industrial period. Figure 10 also indicates that in recent years after the BC
309 concentrations returned to their pre-industrial levels, the peaks once again occurred in summer. During the transition period
310 between the pre-industrial and the peak anthropogenic periods, and that between the peak anthropogenic period and recent
311 years, concentrations show complex seasonal variability. For example, in some years, peaks occurred in both summer and
312 winter/early spring, whereas seasonal peaks were obscured or summer peaks and winter/early spring peaks appeared alternately
313 in other years.
314

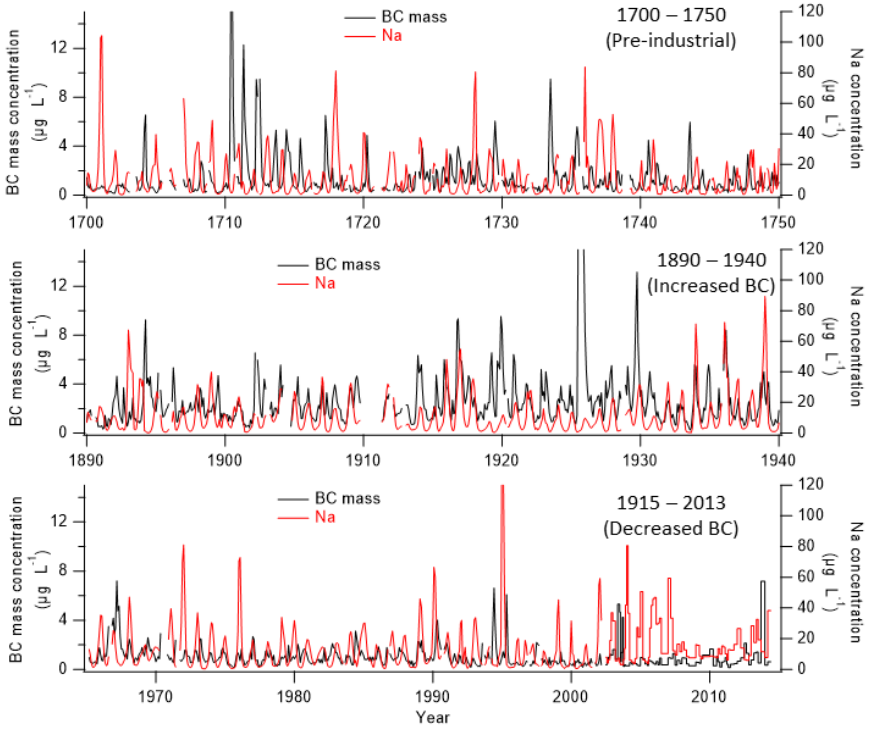

Figure 10: Monthly mean BC mass concentrations and Na concentrations in three periods calculated from the CFA data, with the exception of 2003–2013 (concentrations for this period are raw data from the discrete samples that were analysed with monthly–bimonthly resolution).

315 To examine the general temporal trends in seasonal variations in BC mass concentrations, we plotted 20-year averages
316 of BC mass concentrations in each month for the years 1653–1992 and we plotted 10-year averages for 1993–2002 (Fig. 11).
317 Up until the 20-year period of 1853–1872, BC mass concentrations were elevated from March to September, peaking in the

https://doi.org/10.5194/egusphere-2024-1498
Preprint. Discussion started: 23 May 2024

318 late-spring to summer months (i.e., May–July). After the 20-year period of 1853–1872, BC concentrations in autumn to spring
319 increased and became dominant. During the first half of the 20th century, BC mass concentrations peaked in the winter months
320 of December and January. The autumn to spring increases in BC concentrations are likely attributable to inflow of
321 anthropogenic emissions (McConnell et al., 2007). The seasonality of the anthropogenic BC at SIGMA-D is consistent with
322 that of the present-day atmospheric BC observations at Arctic sites such as Alert (Canadian high Arctic), Ny-Alesund
323 (Svalbard), Barrow (Alaska), and a Greenland coastal site (Sharma et al., 2006, 2019; Gong et al., 2010; Qi and Wang, 2019;
324 Massling et al., 2015).

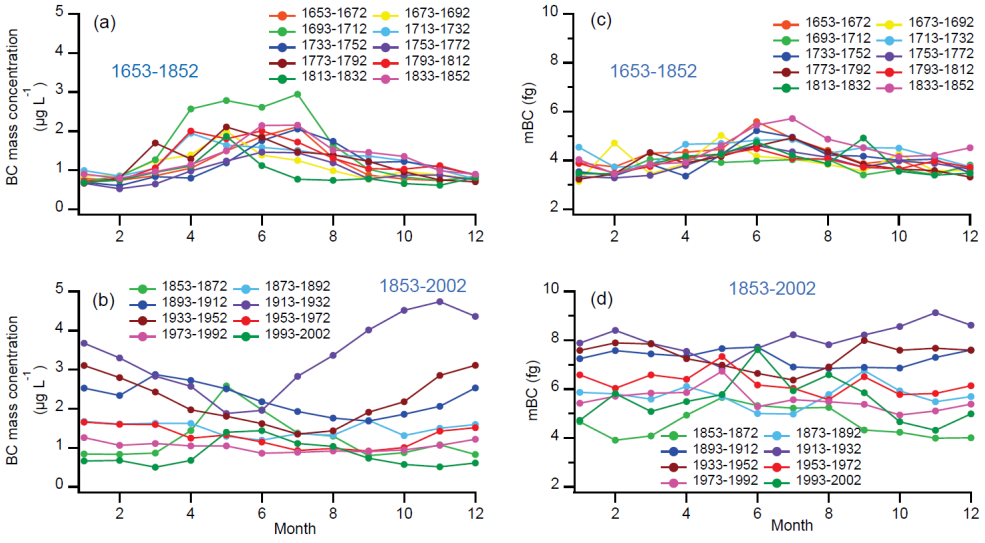

Figure 11: Twenty-year averages of (a) and (b) BC mass concentrations and (c) and (d) mBC in each month for the years 1653–1992 and the 10-year averages for 1993–2002.

325

326 After the 20-year period of 1913–1933, when the anthropogenic input was at its maximum, the autumn to spring
327 concentrations decreased. During 1993–2002, the BC mass concentration peaked in summer again. The recent seasonality of
328 BC at the SIGMA-D site is the same as that observed at other Greenland ice-coring sites, including EGRIP (Du et al., 2020)
329 and Summit (Fig. 1) (Schmeisser et al., 2018), but it differs from that of atmospheric observations in the Arctic (including
330 Greenland), where BC concentrations peak in winter/early spring (Sharma et al., 2006, 2019; Gong et al., 2010; Qi and Wang,
331 2019; Massling et al., 2015). Although we do not present the results for BC number concentrations, they showed seasonal

https://doi.org/10.5194/egusphere-2024-1498
Preprint. Discussion started: 23 May 2024

variations similar to those found in mass concentrations. The influence of anthropogenic emissions in the recent two decades appears to be much lower at the ice coring sites of SIGMA-D, EGRIP, and Summit, located at elevations of >2000 m a.s.l., in comparison with that at atmospheric observation sites located near sea level where anthropogenic emissions remain dominant. At the high-elevation sites on the GrIS, concentrations of BC from biomass burning have exceeded those associated with anthropogenic emissions since the late 20th century, which is likely attributable to reduced emissions of anthropogenically derived BC, primarily in NA and secondarily in EU (McConnell, 2010; McConnell et al., 2007; Moseid et al., 2022).

To understand the general temporal trends in seasonal variations in BC size, we plotted 20-year averages of mBC in each month for the years of 1653–1992 and we plotted 10-year averages for 1993–2002 (Fig. 11). Up until the 20-year period of 1853–1872, mBC peaked in spring to the summer months (May–July) in most of the 20-year periods and it never peaked in the winter months. After the 20-year period of 1873–1892, mBC in autumn–spring increased and its seasonality became obscured. After the peak anthropogenic period of 1913–1933, mBC in autumn–spring decreased. During 1993–2002, mBC once again peaked in summer. We see similar temporal trends in Fig. 12, i.e., both MMD and mBC showed higher values in summer in the pre-industrial period. This seasonality would indicate that the sizes of BC particles originated from biomass burning are greater in summer than in winter. The winter and summer values started to increase in the 1830s–1840s with larger rates of increase for winter values. Winter and summer values both peaked in the 1910s–1940s and subsequently decreased, with similar rates for winter and summer. During the peak anthropogenic period, the summer and winter values were close, which obscured the seasonality in BC particle size (Fig. 11(b)). The winter values became lower than the summer values in 1993–2002. Larger BC particles in winter in the anthropogenic period support the argument that BC particles deposited at SIGMA-D were larger when originating from anthropogenic emissions than when associated with biomass burning.

In the pre-industrial period, biomass burning would have been the predominant source of BC. Backward trajectory analyses (Figs. 6 and 7) indicate that boreal forest fires in NA would be the primary sources of BC in summer at both the SIGMA-D site and the D4 site. Although the contributions of air masses from RUS are very small, especially in summer (<3% at SIGMA-D; <1% at D4), Siberia has also been proposed as a potential source of pyrogenic aerosols to Greenland (Zennaro et al., 2014). A recent study using the CAM-ATRAS global climate–aerosol model (Matsui et al., 2022) showed that Siberia has made the largest contribution to BC concentrations found in the recent Arctic snow, although the contribution to Greenland snow specifically has not been reported. We speculate that biomass burning in Siberia could be a secondary source of BC at the SIGMA-D site in summer because the backward trajectory analyses showed that air masses originated from Siberia (Fig.

https://doi.org/10.5194/egusphere-2024-1498
Preprint. Discussion started: 23 May 2024

359 7). In winter, the boreal forests in NA and Siberia are covered with snow and thus there is little contribution of BC from boreal
360 forest fires (Bond et al., 2013). However, BC concentrations are not zero, even in winter. Biomass burning in lower latitudes
361 (Zennaro et al., 2014) could be a source of BC in winter, and the smaller sizes of BC particles in pre-industrial winter periods
362 suggest long-range transport of BC that supports this assumption.
363

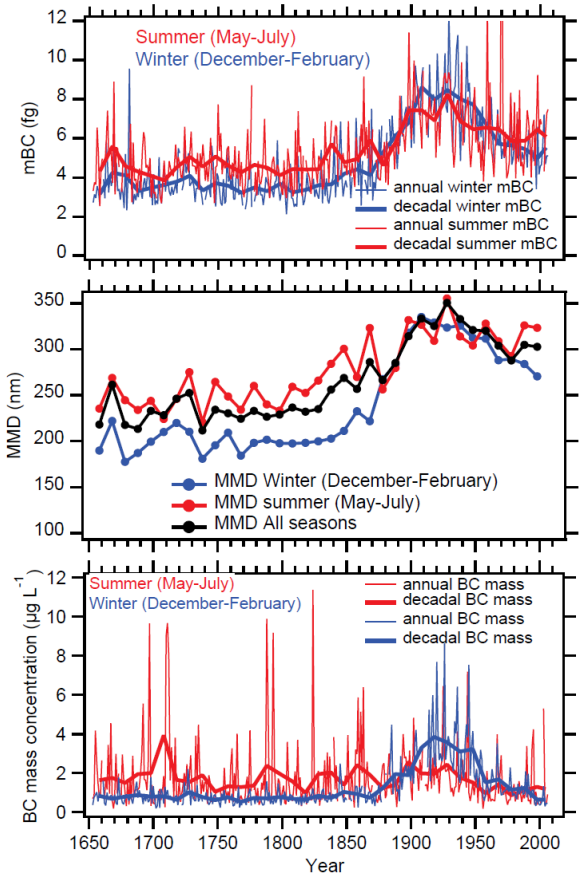

Figure 12: (a) Annual and decadal means of winter (December–February) and summer (May–July) mBC, (b) decadal means of winter, summer, and all-season (January–December) MMD, and (c) annual and decadal means of winter and summer BC mass concentrations. In all panels, thin and thick solid lines denote annual and decadal means, respectively. Blue, red, and black curves denote winter, summer, and all-season means, respectively.

364 **3.3 Historical changes in BC originated from biomass burning**

https://doi.org/10.5194/egusphere-2024-1498
Preprint. Discussion started: 23 May 2024

Figure 13 presents monthly mean BC mass concentrations for the past 350 years, together with NH_4^+ concentrations. Occasional high peaks in summer likely originated from large boreal forest fires, mainly in NA but with possible additional contributions from Siberia. Many of the high BC peaks in summer coincide with high NH_4^+ concentration peaks in summer, which originate from large boreal forest fires (e.g., Legrand et al., 2016). Table A1 lists the biomass burning events distinguished in the record of the SIGMA-D ice core, and in other ice cores and the surface snow of Greenland. The events distinguished in the SIGMA-D core were defined using BC mass concentration peaks and NH_4^+ concentration peaks. For BC, peaks exceeding the summer (May–July) averages for 350 years + 2σ or 3σ were selected, whereas for NH_4^+, summer peaks exceeding the annual averages for 350 years + 2σ or 3σ were selected. If a BC or NH_4^+ summer peak in the SIGMA-D core with a concentration between the average + 1σ and 2σ was found in the same year as when a large biomass burning event was recorded at other Greenland sites, we also selected that peak as a biomass burning event. If the year of a biomass burning event reported by previous studies agreed with that in the SIGMA-D core to within ±2 years, taking account of dating errors in different ice cores, we assumed that the record in the different cores reflected the same event. In Fig. 13(b), we marked only those events exceeding the average + 3σ. Most of the marked events (peaks in 1655, 1665, 1697, 1710, 1711, 1712, 1733, 1788, 1793, 1824, 1851, 1859, 1863, 1925, and 1944) occurred in May, June, or July; however, those in 1789, 1812, and 1894 occurred in April, the one in 1773 occurred in September, and the one in 1929 occurred in August. The peaks in 1925 and 1944 occurred in May and June, and we assumed that they originated from large biomass burning events. Nevertheless, we could not abandon the possibility that these summer peaks might have been affected by large peaks in the preceding winters owing to signal dispersion in the CFA system.

Most of the large events with BC concentrations that exceeded the average + 3σ were also recorded in boreal forest fire records reconstructed from BC, NH_4^+, or levoglucosan concentrations in other Greenland ice cores (Table A1). The high BC concentration peaks in the summers of 1665, 1710, 1711, 1712, 1812, and 1824, accompanying high NH_4^+ peaks, and the high BC peak in 1859 have not been reported previously. The high NH_4^+ concentration peaks in 1675, 1690, and 1750 have no corresponding BC peaks in April, May, June, July, or August, while those in 1675, 1710, 1712, 1715, and 1761 do have corresponding BC peaks. As for the NH_4^+ concentration peak in 1690, the summer BC data were missing and therefore comparison was not possible. Although Keegan et al. (2014) argued that the high summer BC concentrations in 1889 and 2012 found at Summit were associated with widespread melt events in Greenland, no high BC concentration peaks were found in 1889 or 2012 at the SIGMA-D site. As shown in Fig. 13 and Table A1, some of the large biomass burning events recorded in

https://doi.org/10.5194/egusphere-2024-1498
Preprint. Discussion started: 23 May 2024

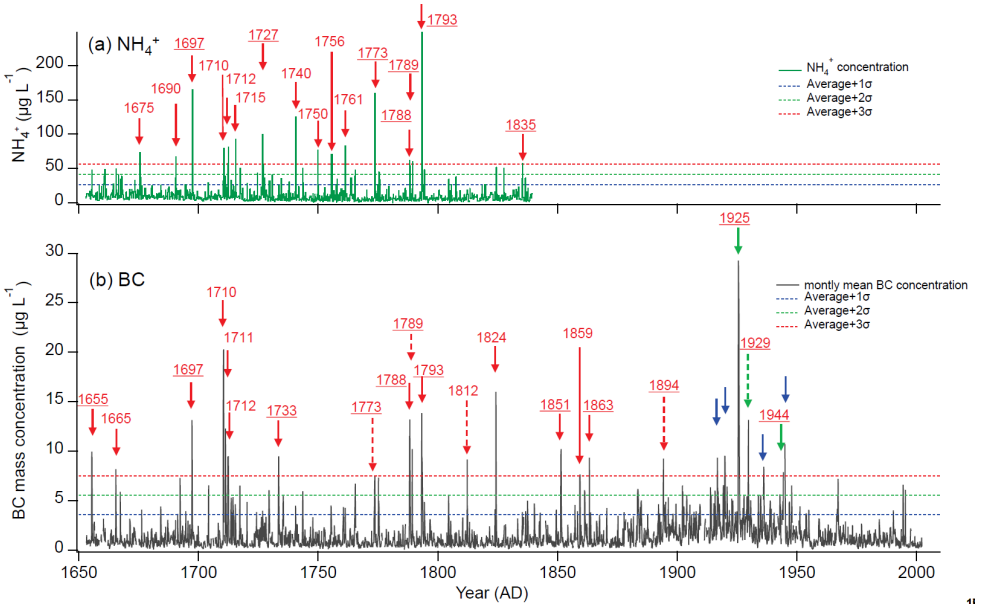

Figure 13: NH_4^+ concentrations: (a) raw data and (b) monthly mean BC mass concentrations (calculated from CFA data. Red arrows in (a) show years when concentrations exceeded the average + 3σ in summer. Solid and broken arrows in (b) show years when concentrations exceeded the summer (May–July) average + 3σ in summer (May–July), and in spring or autumn months (April, August, and September), respectively. Blue arrows in (b) show years when concentrations exceeded the summer average + 3σ in winter. Solid and broken green arrows in (b) show years when concentrations exceeded the summer (May–July) average + 3σ in summer (May–July), and in spring or autumn months (April, August, and September), respectively, but those that might have been affected by winter peaks. Underlining denotes years when biomass burning events were also recorded in other Greenland ice cores/surface snow samples within 2 years. Dotted lines in (a) denote the concentration average over 350 years + 1σ (blue), + 2σ (green), and +3σ (red). Dotted lines in (b) denote summer (May–July) concentration average over 350 years + 1σ (blue), + 2σ (green), and +3σ (red).

392 other Greenland ice cores were not recorded in the SIGMA-D core, and vice versa. There are two possible reasons for this: (1)
393 different ice core sites are not always on the transport pathways of BC from boreal forest fires (Legrand et al., 2016), and (2)
394 wind scour at a site can remove snow containing high concentrations of BC. Despite the minor regional differences within
395 Greenland, most of the large BC concentration peaks caused by large biomass burning events were recorded widely across
396 Greenland. This indicates that high BC concentration peaks could be used to synchronize different ice cores in Greenland as

https://doi.org/10.5194/egusphere-2024-1498
Preprint. Discussion started: 23 May 2024

397 reference horizons for dating, as is usually carried out with volcanic sulphate peaks and their signatures detected by
398 DEP(dielectric profiling) and ECM (electrical conductivity measurement) peaks (Rasmussen et al., 2008; Sinnl et al., 2022).
399 The numbers of large biomass burning events in each 10 years are plotted in Fig. 14 using different definitions of a
400 "large" event. Figure 14(a) displays the numbers of months with mass concentrations in summer (May–July) exceeding the
401 summer average + 1σ, 2σ, and 3σ; Fig. 14(b) displays the number of months with number concentrations in summer exceeding
402 the summer average + 1σ, 2σ, and 3σ. Because large events in April, August, and September were not counted to avoid the
403 potential for impact of anthropogenic BC, there would be minor underestimation of the number of large events. Although the
404 frequency of large events differs slightly between the different definitions, the general tendency is consistent. Large events
405 tended to be more frequent around the 1710s, 1790s, 1850s, 1900s, and 1950s. Moreover, there is no obvious trend of increase
406 up to the decade 1993–2002. To study the historical trends in concentrations of BC originated from biomass burning, we
407 calculated the decadal averages of BC mass and number concentrations for each month (Fig. 15). During the pre-industrial
408 period, both mass and number concentrations were stable in the winter months (December–February), whereas they showed

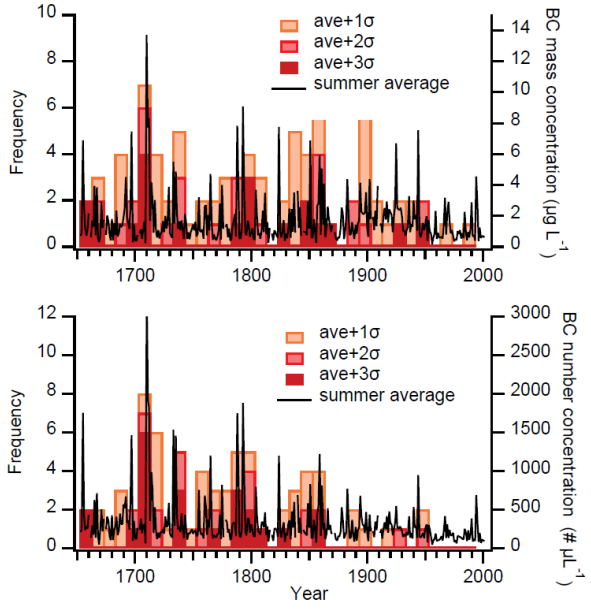

Figure 14: Frequency of large biomass burning events. Black curves denote summer (May–July) averages of BC concentrations. Bars show frequency of BC summer peaks in each decade exceeding the average + 1σ, 2σ, and 3σ. (a) Mass concentrations of BC were used to define peaks. (b) Number concentrations of BC were used to define peaks.

https://doi.org/10.5194/egusphere-2024-1498
Preprint. Discussion started: 23 May 2024

409 large inter-decadal fluctuations in spring to autumn months (March–November). The fluctuations appear largest in spring–
410 summer (April–July). Generally, the period of April–July is likely when the occurrence of large boreal forest fires increases
411 in NA (Whitman et al., 2018). The sporadic nature of the frequency of occurrence of large boreal forest fires would explain
412 the large fluctuations.

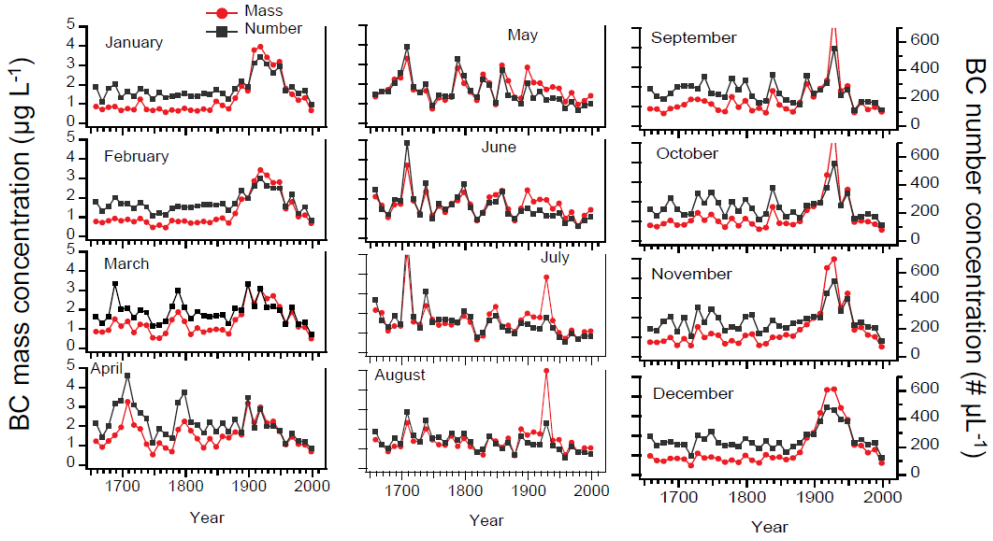

Figure 15: Decadal averages of BC mass (red) and number (black) concentrations for each month.

413 Since the 1870s, when anthropogenic BC started to influence the SIGMA-D site, BC mass and number concentrations
414 in September–April increased, as discussed in Sect. 3.3; however, there was little increase during the spring–summer months.
415 Although large inter-decadal variability in concentrations during spring–summer obscured the temporal trends in spring–
416 summer concentrations (Fig. 11), the general temporal trends are more apparent in Fig. 15. At the SIGMA-D site, we see slight
417 trends of reduction in BC mass and number concentrations during spring–summer. Analysis of Fig. 14 also suggests that the
418 frequency of large boreal forest fires in NA showed a slight trend of reduction over the past 350 years until the most recent
419 decade (1993–2002). However, this trend has not been reported by previous studies on other ice cores from Greenland, partly
420 owing to the different periods covered, the different temporal resolution of the analysis methods, and the different fire proxies
421 used (Zennaro et al., 2014; Legrand et al., 2016; Parvin et al., 2019; Savarino and Legrand, 1998; Whitlow et al., 1994). Most
422 previous studies used NH_4^+ as a fire proxy, with occasional use of levoglucosan and other organic materials; only a few studies
423 have used BC as a fire proxy for pre-industrial periods (Zennaro et al., 2014).

https://doi.org/10.5194/egusphere-2024-1498
Preprint. Discussion started: 23 May 2024

Since the 1950s, data on the area burned and the number of forest fires in Canada have become available (Hanes et al., 2018; Skakun et al., 2021). The SIGMA-D record does not appear to trace the Canadian forest fire database. Air masses arriving at the SIGMA-D site might not have passed over Canada during periods of large forest fires. Large uncertainties in fire data might also explain the disagreement. There are also large uncertainties and regional variability in sedimentary charcoal fire records (Marlon et al., 2012, 2013; Power et al., 2013). However, our results are consistent with the charcoal data from western NA, which show general decline in biomass burning since 1500, with a relatively enhanced fire period in the mid-19th century (Power et al., 2013). The biomass burning emission inventories for CMIP 6 also have large uncertainties (van Marle et al., 2017). Therefore, much more work is needed on the reconstruction of past biomass burning using ice cores.

3.4 Impacts of BC on the ice sheet albedo

McConnell et al. (2007) calculated the quantitative impacts of BC in snow on radiative forcing during early summer using BC concentration from D4 ice core and the Snow, Ice, and Aerosol Radiative (SNICAR) model (Flanner et al., 2007), assuming an effective snow grain radius of 100 μm. They estimated the radiative forcing of 1.02 Wm^{-2} during the peak 5-year period from 1906 to 1910, which is a fivefold increase from preindustrial conditions. However, the radiative forcing of BC in snow varies depending on both the assumed solar irradiance and snow grain size. Then, we calculated the possible albedo reduction due to BC at the SIGMA-D site from the monthly mean BC mass concentration data obtained in this study (Fig. 16) using a physically based snow albedo model (Aoki et al., 2011). As the snow albedo reduction rate due to light absorbing particles is enhanced with an increase of snow grain size (Wiscombe and Warren, 1980), we assumed two effective snow grain radii r_s = 50 μm and 1000 μm, corresponding to new snow (defined as 'precipitation particles' according to Fierz et al., 2009) and old melting snow (defined as 'melt forms' according to Fierz et al., 2009) (Wiscombe and Warren, 1980) for clear sky and cloudy sky (overcast) conditions. The albedo reductions under the cloudy sky are 20-48% larger than those under clear sky. These increases are related to the following two factors: 1) the visible albedo depends on BC concentration more strongly than the near infrared albedo (Wiscombe and Warren, 1980); 2) the visible spectral fraction in solar irradiance at the snow surface under cloudy sky is larger than that under clear sky (Aoki et al., 1999). Thus, the albedo reduction due to BC under cloudy sky is enhanced more than clear sky.

Figure 16 demonstrates that the albedo reduction in case of new snow is consistently less than 0.01, even at the maximum value for cloudy conditions in August 1925 (Fig. 16a). In contrast, for old melting snow, the albedo reduction

https://doi.org/10.5194/egusphere-2024-1498
Preprint. Discussion started: 23 May 2024

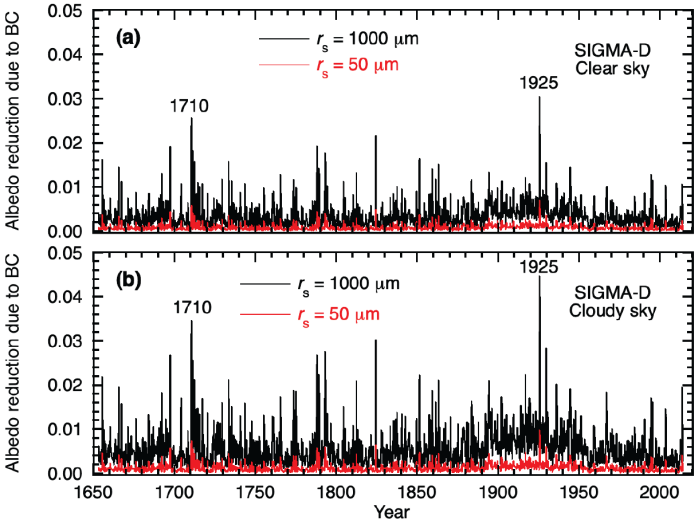

Figure 16: Temporal variation of albedo reduction for (a) clear sky and (b) cloudy sky conditions, calculated from monthly mean BC mass concentrations, for two effective snow grain radii: r_s = 50 μm (representing new snow, indicated by the red line) and r_s = 1000 μm (indicating old melting snow, shown by the black line). The albedo reduction values are calculated for solar zenith angle at local solar noon on the 15th of each month, excluding the polar night period from November to February. The maximum albedo reduction is simulated in 1925 and followed by 1710.

451 frequently exceeds 0.01 for both sky conditions (Fig. 16b). The maximum albedo reduction for cloudy conditions is 0.045 (r_s
452 = 1000 μm) and 0.0098 (r_s = 50 μm) in August 1925, followed by the values of 0.034 (r_s = 1000 μm) and 0.0074 (r_s = 50 μm)
453 in July 1710. The averaged albedo reduction for the overall period of 1650-2014 is 0.0031 (r_s = 1000 μm) and 0.0007 (r_s = 50
454 μm) for clear conditions, and 0.0054 (r_s = 1000 μm) and 0.0011 (r_s = 50 μm) for cloudy conditions. During the anthropogenic
455 concentration peak period of 1913-1933, the average albedo reduction increases to 0.0056 (r_s = 1000 μm) and 0.0012 (r_s = 50
456 μm) for clear conditions, and 0.0089 (r_s = 1000 μm) and 0.0019 (r_s = 50 μm) for cloudy conditions.

457 Warren et al. (2019) described that a BC concentration of 20 parts per billion in weight can cause broadband snow
458 albedo reductions of 1-2%. They also noted that for a typical daily average solar irradiance of 400 W m^{-2} in the Arctic during
459 late spring and early summer, a 1% albedo reduction can lead to a positive forcing of 4 W m^{-2} locally, similar to the forcing
460 caused by doubling CO_2. Our calculation results indicate that a 1% of reduction in albedo can occur at numerous local spike-
461 like peaks for r_s = 1000 μm including the recent several decades after 1950. During the anthropogenic concentration peak

https://doi.org/10.5194/egusphere-2024-1498
Preprint. Discussion started: 23 May 2024

period (1913-1933), the average albedo reduction approaches 1% (0.0089) for r_s = 1000 μm under cloudy sky conditions. Consequently, our simulations suggest that the amount of albedo reduction remains relatively small as long as new snow conditions are maintained. However, if the surface snow grains are the size of old melting snow, which would have occurred during summer months at the SIGMA-D site, the extent of albedo reduction becomes non-negligible.

4 Conclusions

We analysed the record of BC over the past 350 years in the SIGMA-D ice core, which was drilled in northwest Greenland. The improved technique for BC measurement (Mori et al., 2016) and the CFA system built at NIPR allowed us to reconstruct high temporal resolution records of the sizes and concentrations of BC particles. Notably, this study marks the first reconstruction of temporal changes in BC size since the pre-industrial period.

The number and mass concentrations of BC started to increase in the 1870s owing to anthropogenic input. The concentrations reached their maxima in the 1910s–1920s, following which they decreased. By the 1960s, BC concentrations had reduced to levels close to or lower than those of the pre-industrial period. The trend of anthropogenic BC at the SIGMA-D site was generally similar to that reported previously for other ice core sites in Greenland, albeit with slight differences. Backward trajectory analyses suggest that the major anthropogenic emission source that affected the SIGMA-D site was NA. However, the backward trajectory analyses did not clearly explain the slight difference in the temporal trends of BC between the SIGMA-D site and the more southerly site D4. Anthropogenic BC was transported to the SIGMA-D site mainly in the winter half of the year, which was deduced by the changes in the seasonality of BC concentrations. The backward trajectory analyses produced consistent results, showing greater contributions from air masses from the industrial regions in NA and EUR in winter.

Pre-industrial BC concentrations peaked in summer. In association with increased anthropogenic input, concentrations increased in winter to early spring, which shifted the annual peak in concentration to winter–early spring. When the anthropogenic input started to decline in the 1930s, concentrations in winter–early spring also decreased, which changed the seasonality of BC concentrations; by the 1990s, BC concentrations peaked in summer once again. This suggests that the major sources of BC in recent years were not anthropogenic emissions but biomass burning. At the SIGMA-D site, BC originated from anthropogenic emissions made only a minor contribution to the BC concentrations in the summer months throughout the past 350 years. This enabled us to examine the temporal variability in biomass burning throughout the past 350

https://doi.org/10.5194/egusphere-2024-1498
Preprint. Discussion started: 23 May 2024

years, especially after the increase in anthropogenically derived BC, which is a topic that has not been addressed by previous studies on BC data from other ice cores in the Arctic.

The size distributions of BC particles have also changed owing to anthropogenic impact. Both MMD and mBC started to increase around the 1830s or 1840s, peaked in the 1910s–1940s when BC concentrations were at their maxima, and started to decline after the 1940s. Increases in MMD and mBC accompanying the increase in BC concentrations suggest that the diameter of BC particles deposited over northwest Greenland were generally larger for anthropogenic BC than for biomass burning BC. The seasonality of MMD and mBC also changed, accompanying the concentration changes. However, in contrast to BC concentrations, neither MMD nor mBC returned to their pre-industrial values; instead, they remained at higher values in the 1960s–2000s.

Pre-industrial BC would have originated mainly from biomass burning. During the winters (December–February) of the pre-industrial period, decadal averages of monthly mean mass and number concentrations were stable, and the sizes of BC particles were smaller than those in summer. This indicates that BC in pre-industrial winters originated from biomass burning in low latitudes where there was no snow cover in winter, and that biomass burning in low latitudes that affected Greenland showed little change during the pre-industrial period. After the inflow of anthropogenic BC started, it became difficult to distinguish biomass burning BC from anthropogenic BC in winter, making it difficult to discuss the temporal changes in BC originated from low-latitude biomass burning in winter. However, we could discuss the temporal changes in boreal forest fires that occur mainly in summer, the season with minimal anthropogenic input.

Sources of pre-industrial BC were likely boreal forest fires primarily in NA. We investigated the temporal trend in the decadal frequency of large boreal forest fire events using high summer peaks of number and mass concentrations of BC. We found no obvious trend of increase in the decadal frequency of large boreal forest fires until the decade of 1993–2002. Furthermore, we found no trends of increase in the decadal averages of monthly mean mass and number concentrations in summer during the past 350 years; we even found a trend of decrease for number concentrations. Although recent large fire events in NA are attributed to global warming (Brown et al., 2023), the effects of global warming do not seem to have left clear imprint in Greenland until the early 2000s. Therefore, we need further investigations using more recent ice core records of BC.

We analysed the temporal variation of potential albedo reduction due to BC at the SIGMA-D site during the past 350 years using a physically based snow albedo model. Albedo reductions under the assumption of consistently new snow grain

https://doi.org/10.5194/egusphere-2024-1498
Preprint. Discussion started: 23 May 2024

size remained below 0.01, even at the peak BC concentration in 1925. Conversely, under the assumption of old melting snow grain size, the albedo reduction frequently exceeded 0.01. Our calculation results reveal that a 1% of reduction in albedo can occur at numerous local spike-like peaks in the case of old melting snow, including the recent several decades after 1950. During the peak period of anthropogenic concentrations (1913-1933), the averaged albedo reduction approaches 1% for old melting snow cases. Consequently, our simulations suggest that the magnitude of albedo reduction remains relatively small as long as new snow conditions are maintained. However, if the surface snow grains are the size of old melting snow, the amount of albedo reduction becomes non-negligible.

Our new high temporal resolution records of BC concentrations and sizes could contribute to evaluation of the impacts of both anthropogenically derived and biomass burning originated BC on Earth's radiation budget, albedo, BC–cloud interactions, and therefore BC–climate interactions. They could also contribute to validation of emission inventories, and aerosol and climate models. High temporal resolution BC data since 2002 are necessary to investigate the impact of global warming on boreal forest fires. Furthermore, high temporal resolution records of BC concentrations and sizes during the early Holocene and the last interglacial period when it was warmer than the present day (NEEM community members, 2013; Vinther et al., 2009) should be obtained for better projections of BC–climate interactions in a future warming world.

Data availability

All the data used in this study will be submitted to the Arctic Data Archive System (ADS) as soon as the manuscript has been published.

Author contributions

KGA designed the study and led the manuscript writing. YOT was responsible for the BC measurements. YOT, MH, RD, and JO performed the CFA analyses of the SIGMA-D core. MH and SM measured the ion concentrations in the discrete samples. KGA, YOT, and KaF analysed the data. KGA, YOT, NM, TM, SO, YK, and MK interpreted the BC data. KoF performed backward trajectory analyses. TA designed and led the ice coring project at SIGMA-D. TA computed the impacts of BC on albedo. All the authors discussed the results.

Competing interests

https://doi.org/10.5194/egusphere-2024-1498
Preprint. Discussion started: 23 May 2024

543 The authors declare that they have no conflict of interest.

544

545 **Acknowledgements**

546 We would like to thank Hideaki Motoyama who drilled the SIGMA-D core, and Yuki Komuro who cut and processed the core
547 in the field. This study has been supported by JSPS KAKENHI (Grant Numbers: JP 22221002, JP23221004, and JP18H04140),
548 the Arctic Challenge for Sustainability (ArCS) Project (Program Grant Number: JPMXD130000000)), the Arctic Challenge
549 for Sustainability II (ArCS II) Project (Program Grant Number: JPMXD1420318865), and the Environment Research and
550 Technology Development Funds (JPMEERF20172003, JPMEERF20202003 and JPMEERF20232001) of the Environmental
551 Restoration and Conservation Agency of Japan. We thank James Buxton MSc, from Edanz (https://jp.edanz.com/ac), for
552 editing a draft of this manuscript.

553

554 **References**

555 Aoki, T., Aoki, T., Fukabori, M., and Uchiyama, A.: Numerical Simulation of the Atmospheric Effects on Snow Albedo with
556 a Multiple Scattering Radiative Transfer Model for the Atmosphere-Snow System, J. Meteorol. Soc. of Japan. Ser. II,
557 77, 595–614, doi:10.2151/jmsj1965.77.2_595, 1999.
558 Aoki, T., Kuchiki, K., Niwano, M., Kodama, Y., Hosaka, M., and Tanaka, T.: Physically based snow albedo model for
559 calculating broadband albedos and the solar heating profile in snowpack for general circulation models, J. Geophys.
560 Res. Atmos., 116, D11114, doi:10.1029/2010JD015507, 2011.
561 Bauer, S. E., Bausch, A., Nazarenko, L., Tsigaridis, K., Xu, B., Edwards, R., Bisiaux, M., and McConnell, J.: Historical and
562 future black carbon deposition on the three ice caps: Ice core measurements and model simulations from 1850 to 2100, J.
563 Geophys. Res.-Atmos., 118, 7948–7961, doi:10.1002/jgrd.50612, 2013.
564 Baumgardner, D., Kok, G., and Raga, G.: Warming of the Arctic lower stratosphere by light absorbing particles, Geophys.
565 Res. Lett., 31, https://doi.org/10.1029/2003GL018883, 2004.
566 Bisiaux, M. M., Edwards, R., McConnell, J. R., Albert, M. R., Anschütz, H., Neumann, T. A., Isaksson, E., and Penner, J. E.:
567 Variability of black carbon deposition to the East Antarctic Plateau, 1800–2000 AD, Atmos. Chem. Phys., 12, 3799–3808,
568 10.5194/acp-12-3799-2012, 2012a.

https://doi.org/10.5194/egusphere-2024-1498
Preprint. Discussion started: 23 May 2024

569 Bisiaux, M. M., Edwards, R., McConnell, J. R., Curran, M. A. J., Van Ommen, T. D., Smith, A. M., Neumann, T. A., Pasteris,
570 D. R., Penner, J. E., and Taylor, K.: Changes in black carbon deposition to Antarctica from two high-resolution ice core
571 records, 1850–2000 AD, Atmos. Chem. Phys., 12, 4107–4115, 10.5194/acp-12-4107-2012, 2012b.
572 Bond, T. C., Doherty, S. J., Fahey, D. W., Forster, P. M., Berntsen, T., DeAngelo, B. J., Flanner, M. G., Ghan, S., Kärcher, B.,
573 Koch, D., Kinne, S., Kondo, Y., Quinn, P. K., Sarofim, M. C., Schultz, M. G., Schulz, M., Venkataraman, C., Zhang, H.,
574 Zhang, S., Bellouin, N., Guttikunda, S. K., Hopke, P. K., Jacobson, M. Z., Kaiser, J. W., Klimont, Z., Lohmann, U., Schwarz,
575 J. P., Shindell, D., Storelvmo, T., Warren, S. G., and Zender, C. S.: Bounding the role of black carbon in the climate system:
576 A scientific assessment, J. Geophys. Res.-Atmos. n/a-n/a, 10.1002/jgrd.50171, 2013.
577 Breider, T. J., Mickley, L. J., Jacob, D. J., Ge, C., Wang, J., Payer Sulprizio, M., Croft, B., Ridley, D. A., McConnell, J. R.,
578 Sharma, S., Husain, L., Dutkiewicz, V. A., Eleftheriadis, K., Skov, H., and Hopke, P. K.: Multidecadal trends in aerosol
579 radiative forcing over the Arctic: Contribution of changes in anthropogenic aerosol to Arctic warming since 1980, J.
580 Geophys. Res.-Atmos., 10.1002/2016JD025321, 2017.
581 Brown, P. T., Hanley, H., Mahesh, A., Reed, C., Strenfel, S. J., Davis, S. J., Kochanski, A. K., and Clements, C. B.: Climate
582 warming increases extreme daily wildfire growth risk in California, Nature, 621, 760–766, 10.1038/s41586-023-06444-3,
583 2023.
584 Calkin, D. E., Barrett, K., Cohen, J. D., Finney, M. A., Pyne, S. J., and Quarles, S. L.: Wildland-urban fire disasters aren't
585 actually a wildfire problem, P. Natl. Acad. Sci., 120, e2315797120, doi:10.1073/pnas.2315797120, 2023.
586 Dibb, J. E., Talbot, R. W., Whitlow, S. I., Shipham, M. C., Winterle, J., McConnell, J., and Bales, R.: Biomass burning
587 signatures in the atmosphere and snow at Summit, Greenland: An event on 5 August 1994, Atmos. Environ., 30, 553–561,
588 10.1016/1352-2310(95)00328-2, 1996.
589 Du, Z.-H., Xiao, C.-D., Dou, T.-F., Li, C.-J., Ding, M.-H., Sharma, S., Ma, X.-Y., Wang, S.-M., and Zhang, W.-B.: A shallow
590 ice core from East Greenland showing a reduction in black carbon during 1990–2016, Adv. Clim. Change Res., 11, 360–
591 369, https://doi.org/10.1016/j.accre.2020.11.009, 2020.
592 Eckhardt, S., Pisso, I., Evangeliou, N., Zwaaftink, C. G., Plach, A., McConnell, J. R., Sigl, M., Ruppel, M., Zdanowicz, C.,
593 Lim, S., Chellman, N., Opel, T., Meyer, H., Steffensen, J. P., Schwikowski, M., and Stohl, A.: Revised historical Northern
594 Hemisphere black carbon emissions based on inverse modeling of ice core records, Nat. Commun., 14, 271,
595 10.1038/s41467-022-35660-0, 2023.

https://doi.org/10.5194/egusphere-2024-1498
Preprint. Discussion started: 23 May 2024

596 Fierz, C., Armstrong, R.L., Durand, Y., Etchevers, P., Greene, E., McClung, D.M., Nishimura, K., Satyawali, P.K. and
597 Sokratov, S.A.: The International Classification for Seasonal Snow on the Ground, IHP-VII Technical Documents in
598 Hydrology N°83, IACS Contribution N°1, UNESCO-IHP, Paris, 2009.
599 Fischer, H., Schupbach, S., Gfeller, G., Bigler, M., Rothlisberger, R., Erhardt, T., Stocker, T. F., Mulvaney, R., and Wolff, E.
600 W.: Millennial changes in North American wildfire and soil activity over the last glacial cycle, Nature Geosci., 8, 723–727,
601 doi:10.1038/ngeo2495, 2015.
602 Flanner, M. G., Zender, C. S., Randerson, J. T., and Rasch, P. J.: Present-day climate forcing and response from black carbon
603 in snow, J. Geophys. Res. 112, doi:10.1029/2006JD008003, 2007.
604 Gong, S. L., Zhao, T. L., Sharma, S., Toom-Sauntry, D., Lavoué, D., Zhang, X. B., Leaitch, W. R., and Barrie, L. A.:
605 Identification of trends and interannual variability of sulfate and black carbon in the Canadian High Arctic: 1981–2007, J.
606 Geophys. Res.-Atmos., 115, https://doi.org/10.1029/2009JD012943, 2010.
607 Goto-Azuma, K. and Koerner, R. M.: Ice core studies of anthropogenic sulfate and nitrate trends in the Arctic, J. Geophys.
608 Res.-Atmos., 106, 4959–4969, 2001.
609 Goto-Azuma, K., Coauthors TBD: Technical note: High-resolution analyses of concentrations and sizes of black carbon
610 particles deposited on northwest Greenland over the past 350 years – Part 1. Continuous flow analysis of the SIGMA-D ice
611 core using a Wide-Range Single-Particle Soot Photometer and a high-efficiency nebulizer, submitted to Atmos. Phys. Chem.
612 Grieman, M. M., Aydin, M., Fritzsche, D., McConnell, J. R., Opel, T., Sigl, M., and Saltzman, E. S.: Aromatic acids in a
613 Eurasian Arctic ice core: a 2600-year proxy record of biomass burning, Clim. Past, 13, 395–410, 10.5194/cp-13-395-2017,
614 2017.
615 Grieman, M. M., Aydin, M., McConnell, J. R., and Saltzman, E. S.: Burning-derived vanillic acid in an Arctic ice core from
616 Tunu, northeastern Greenland, Clim. Past, 14, 1625–1637, 10.5194/cp-14-1625-2018, 2018.
617 Hanes, C. C., Wang, X., Jain, P., Parisien, M.-A., Little, J. M., and Flannigan, M. D.: Fire-regime changes in Canada over the
618 last half century, Can. J. Forest Res., 49, 256–269, 10.1139/cjfr-2018-0293, 2018.
619 Hennigan, C. J., Sullivan, A. P., Collett Jr., J. L., and Robinson, A. L.: Levoglucosan stability in biomass burning particles
620 exposed to hydroxyl radicals, Geophys. Res. Lett., 37, https://doi.org/10.1029/2010GL043088, 2010.
621 Hersbach, H., Bell, B., Berrisford, P., Hirahara, S., Horányi, A., Muñoz-Sabater, J., Nicolas, J., Peubey, C., Radu, R., Schepers,
622 D., Simmons, A., Soci, C., Abdalla, S., Abellan, X., Balsamo, G., Bechtold, P., Biavati, G., Bidlot, J., Bonavita, M., De

https://doi.org/10.5194/egusphere-2024-1498
Preprint. Discussion started: 23 May 2024

Chiara, G., Dahlgren, P., Dee, D., Diamantakis, M., Dragani, R., Flemming, J., Forbes, R., Fuentes, M., Geer, A., Haimberger, L., Healy, S., Hogan, R. J., Hólm, E., Janisková, M., Keeley, S., Laloyaux, P., Lopez, P., Lupu, C., Radnoti, G., de Rosnay, P., Rozum, I., Vamborg, F., Villaume, S., and Thépaut, J.-N.: The ERA5 global reanalysis, Q. J. Roy. Meteor. Soc., 146, 1999–2049, https://doi.org/10.1002/qj.3803, 2020.

Hoesly, R. M., Smith, S. J., Feng, L., Klimont, Z., Janssens-Maenhout, G., Pitkanen, T., Seibert, J. J., Vu, L., Andres, R. J., Bolt, R. M., Bond, T. C., Dawidowski, L., Kholod, N., Kurokawa, J. I., Li, M., Liu, L., Lu, Z., Moura, M. C. P., O'Rourke, P. R., and Zhang, Q.: Historical (1750–2014) anthropogenic emissions of reactive gases and aerosols from the Community Emissions Data System (CEDS), Geosci. Model Dev., 11, 369–408, 10.5194/gmd-11-369-2018, 2018.

Jurányi, Z., Zanatta, M., Lund, M. T., Samset, B. H., Skeie, R. B., Sharma, S., Wendisch, M., and Herber, A.: Atmospheric concentrations of black carbon are substantially higher in spring than summer in the Arctic, Comm. Earth Environ., 4, 91, 10.1038/s43247-023-00749-x, 2023.

Kaspari, S. D., Schwikowski, M., Gysel, M., Flanner, M. G., Kang, S., Hou, S., and Mayewski, P. A.: Recent increase in black carbon concentrations from a Mt. Everest ice core spanning 1860–2000 AD, Geophys. Res. Lett., 38, L04703, 10.1029/2010gl046096, 2011.

Kawamura, K., Izawa, Y., Mochida, M., and Shiraiwa, T.: Ice core records of biomass burning tracers (levoglucosan and dehydroabietic, vanillic and p-hydroxybenzoic acids) and total organic carbon for past 300 years in the Kamchatka Peninsula, Northeast Asia, Geochim. Cosmoshim. Acta, 99, https://doi.org/10.1016/j.gca.2012.08.006 317-329, 2012.

Keane, R. E., Agee, J. K., Fulé, P., Keeley, J. E., Key, C., Kitchen, S. G., Miller, R., and Schulte, L. A.: Ecological effects of large fires on US landscapes: benefit or catastrophe? Int. J. Wildland Fire, 17, 696–712, https://doi.org/10.1071/WF07148, 2008.

Keegan, K. M., Albert, M. R., McConnell, J. R., and Baker, I.: Climate change and forest fires synergistically drive widespread melt events of the Greenland Ice Sheet, P. Natl. Acad. Sci., 111, 7964–7967, 10.1073/pnas.1405397111, 2014.

Keeley, J. E. and Syphard, A. D.: Large California wildfires: 2020 fires in historical context, Fire Ecology, 17, 22, 10.1186/s42408-021-00110-7, 2021.

Kehrwald, N., Zangrando, R., Gabrielli, P., Jaffrezo, J.-L., Boutron, C., Barbante, C., and Gambaro, A.: Levoglucosan as a specific marker of fire events in Greenland snow, Tellus B: Chem. Phys. Meteorol., 64, 18196, 10.3402/tellusb.v64i0.18196, 2012.

https://doi.org/10.5194/egusphere-2024-1498
Preprint. Discussion started: 23 May 2024

650 Lamarque, J. F., Bond, T. C., Eyring, V., Granier, C., Heil, A., Klimont, Z., Lee, D., Liousse, C., Mieville, A., Owen, B.,
651 Schultz, M. G., Shindell, D., Smith, S. J., Stehfest, E., Van Aardenne, J., Cooper, O. R., Kainuma, M., Mahowald, N.,
652 McConnell, J. R., Naik, V., Riahi, K., and van Vuuren, D. P.: Historical (1850–2000) gridded anthropogenic and biomass
653 burning emissions of reactive gases and aerosols: methodology and application, Atmos. Chem. Phys., 10, 7017–7039,
654 10.5194/acp-10-7017-2010, 2010.
655 Legrand, M. and De Angelis, M.: Light carboxylic acids in Greenland ice: A record of past forest fires and vegetation emissions
656 from the boreal zone, J. Geophys. Res.-Atmos., 101, 4129–4145, https://doi.org/10.1029/95JD03296, 1996.
657 Legrand, M. and Mayewski, P.: Glaciochemistry of polar ice cores: A review, Rev. Geophys., 35, 219–243,
658 10.1029/96RG03527, 1997.
659 Legrand, M., De Angelis, M., Staffelbach, T, Neftel, A., and Stauffer, B.: Large perturbations of ammonium and organic acids
660 in the Summit-Greenland ice core. Fingerprint from forest fires? Geophys. Res. Lett., 19, 473-475,
661 http://dx.doi.org/10.1029/91GL03121, 1992.
662 Legrand, M., McConnell, J., Fischer, H., Wolff, E. W., Preunkert, S., Arienzo, M., Chellman, N., Leuenberger, D., Maselli,
663 O., Place, P., Sigl, M., Schüpbach, S., and Flannigan, M.: Boreal fire records in Northern Hemisphere ice cores: A review,
664 Clim. Past, 12, 2033–2059, 10.5194/cp-12-2033-2016, 2016.
665 Marlon, J. R., Bartlein, P. J., Gavin, D. G., Long, C. J., Anderson, R. S., Briles, C. E., Brown, K. J., Colombaroli, D., Hallett,
666 D. J., Power, M. J., Scharf, E. A., and Walsh, M. K.: Long-term perspective on wildfires in the western USA, P. Natl. Acad.
667 Sci., 109, E535–E543, 10.1073/pnas.1112839109, 2012.
668 Marlon, J. R., Bartlein, P. J., Daniau, A.-L., Harrison, S. P., Maezumi, S. Y., Power, M. J., Tinner, W., and Vanniére, B.:
669 Global biomass burning: a synthesis and review of Holocene paleofire records and their controls, Quaternary Sci. Rev., 65,
670 5–25, http://dx.doi.org/10.1016/j.quascirev.2012.11.029, 2013.
671 Marlon, J. R., Kelly, R., Daniau, A. L., Vannière, B., Power, M. J., Bartlein, P., Higuera, P., Blarquez, O., Brewer, S., Brücher,
672 T., Feurdean, A., Romera, G. G., Iglesias, V., Maezumi, S. Y., Magi, B., Courtney Mustaphi, C. J., and Zhihai, T.:
673 Reconstructions of biomass burning from sediment-charcoal records to improve data–model comparisons, Biogeosciences,
674 13, 3225–3244, 10.5194/bg-13-3225-2016, 2016.

https://doi.org/10.5194/egusphere-2024-1498
Preprint. Discussion started: 23 May 2024

675 Massling, A., Nielsen, I. E., Kristensen, D., Christensen, J. H., Sørensen, L. L., Jensen, B., Nguyen, Q. T., Nøjgaard, J. K.,
676 Glasius, M., and Skov, H.: Atmospheric black carbon and sulfate concentrations in Northeast Greenland, Atmos. Chem.
677 Phys., 15, 9681–9692, 10.5194/acp-15-9681-2015, 2015.
678 Matoba, S., Motoyama, H., Fujita, K., Yamasaki, T., Minowa, M., Onuma, Y., Komuro, Y., Aoki, T., Yamaguchi, S.,
679 Sugiyama, S., and Enomoto, H.: Glaciological and meteorological observations at the SIGMA-D site, northwestern
680 Greenland Ice Sheet, B. Glaciol. Res., 33, 7–14, 10.5331/bgr.33.7, 2015.
681 Matsui, H., Mori, T., Ohata, S., Moteki, N., Oshima, N., Goto-Azuma, K., Koike, M., and Kondo, Y.: Contrasting source
682 contributions of Arctic black carbon to atmospheric concentrations, deposition flux, and atmospheric and snow radiative
683 effects, Atmos. Chem. Phys., 22, 8989–9009, 10.5194/acp-22-8989-2022, 2022.
684 McConnell, J. R.: New Directions: Historical black carbon and other ice core aerosol records in the Arctic for GCM evaluation,
685 Atmos. Environ., 44, 2665–2666, https://doi.org/10.1016/j.atmosenv.2010.04.004, 2010.
686 McConnell, J. R., Edwards, R., Kok, G. L., Flanner, M. G., Zender, C. S., Saltzman, E. S., Banta, J. R., Pasteris, D. R., Carter,
687 M. M., and Kahl, J. D.: 20th-century industrial black carbon emissions altered Arctic climate forcing, Science, 317, 1381–
688 1384, 10.1126/science.1144856, 2007.
689 Mori, T., Moteki, N., Ohata, S., Koike, M., Goto-Azuma, K., Miyazaki, Y., and Kondo, Y.: Improved technique for measuring
690 the size distribution of black carbon particles in liquid water, Aerosol Sci. Tech., 50, 242–254,
691 10.1080/02786826.2016.1147644, 2016.
692 Mori, T., Goto-Azuma, K., Kondo, Y., Ogawa-Tsukagawa, Y., Miura, K., Hirabayashi, M., Oshima, N., Koike, M., Kupiainen,
693 K., Moteki, N., Ohata, S., Sinha, P. R., Sugiura, K., Aoki, T., Schneebeli, M., Steffen, K., Sato, A., Tsushima, A., Makarov,
694 V., Omiya, S., Sugimoto, A., Takano, S., and Nagatsuka, N.: Black Carbon and Inorganic Aerosols in Arctic Snowpack, J.
695 Geophys. Res.-Atmos., 124, 13325–13356, 10.1029/2019jd030623, 2019.
696 Moseid, K. O., Schulz, M., Eichler, A., Schwikowski, M., McConnell, J. R., Olivié, D., Criscitiello, A. S., Kreutz, K. J., and
697 Legrand, M.: Using ice cores to evaluate CMIP6 aerosol concentrations over the historical era, J. Geophys. Res.-Atmos.,
698 127, e2021JD036105, https://doi.org/10.1029/2021JD036105, 2022.
699 Mosher, B. W., Winkler, P., and Jaffrezo, J.-L.: Seasonal aerosol chemistry at Dye 3, Greenland, Atmos. Environ. A-Gen., 27,
700 2761–2772, https://doi.org/10.1016/0960-1686(93)90308-L, 1993.

https://doi.org/10.5194/egusphere-2024-1498
Preprint. Discussion started: 23 May 2024

Moteki, N.: Climate-relevant properties of black carbon aerosols revealed by in situ measurements: a review, Prog. Earth Planet. Sci., 10, 12, 10.1186/s40645-023-00544-4, 2023.

Nagatsuka, N., Goto-Azuma, K., Tsushima, A., Fujita, K., Matoba, S., Onuma, Y., Dallmayr, R., Kadota, M., Hirabayashi, M., Ogata, J., Ogawa-Tsukagawa, Y., Kitamura, K., Minowa, M., Komuro, Y., Motoyama, H., and Aoki, T.: Variations in mineralogy of dust in an ice core obtained from northwestern Greenland over the past 100 years, Clim. Past, 17, 1341–1362, 10.5194/cp-17-1341-2021, 2021.

Nagatsuka, N., Goto-Azuma, K., Fujita, K., Komuro, Y., Hirabayashi, M., Ogata, J., Fukuda, K., Ogawa-Tsukagawa, Y., Kitamura, K., Yonekura, A., Nakazawa, F., Onuma, Y., Kurita, N., Rasmussen, S. O., Sinnl, G., Popp, T. J., and Dahl-Jensen, D.: Regional variations in mineralogy of dust in ice cores obtained from northeastern and northwestern Greenland over the past 100 years, EGUsphere, 2023, 1–32, 10.5194/egusphere-2023-1666, 2023.

Neem Community Members: Eemian interglacial reconstructed from a Greenland folded ice core, Nature, 493, 489–494, 10.1038/nature11789, 2013.

Ohata, S., Moteki, N., Schwarz, J., Fahey, D., and Kondo, Y.: Evaluation of a method to measure black carbon particles suspended in rainwater and snow samples, Aerosol Sci. Technol., 47, 1073–1082, 10.1080/02786826.2013.824067, 2013.

Osmont, D., Wendl, I. A., Schmidely, L., Sigl, M., Vega, C. P., Isaksson, E., and Schwikowski, M.: An 800-year high-resolution black carbon ice core record from Lomonosovfonna, Svalbard, Atmos. Chem. Phys., 18, 12777–12795, 10.5194/acp-18-12777-2018, 2018.

Parvin, F., Seki, O., Fujita, K., Iizuka, Y., Matoba, S., Ando, T., and Sawada, K.: Assessment for paleoclimatic utility of biomass burning tracers in SE-Dome ice core, Greenland, Atmos. Environ., 196, 86–94, https://doi.org/10.1016/j.atmosenv.2018.10.012, 2019.

Pokhrel, A., Kawamura, K., Kunwar, B., Ono, K., Tsushima, A., Seki, O., Matoba, S., and Shiraiwa, T.: Ice core records of levoglucosan and dehydroabietic and vanillic acids from Aurora Peak in Alaska since the 1660s: A proxy signal of biomass-burning activities in the North Pacific Rim, Atmos. Chem. Phys., 20, 597–612, 10.5194/acp-20-597-2020, 2020.

Power, M. J., Marlon, J. R., Bartlein, P. J., and Harrison, S. P.: Fire history and the Global Charcoal Database: A new tool for hypothesis testing and data exploration, Palaeogeogr. Palaeocl., 291, 52–59, http://dx.doi.org/10.1016/j.palaeo.2009.09.014, 2010.

https://doi.org/10.5194/egusphere-2024-1498
Preprint. Discussion started: 23 May 2024

Power, M., Mayle, F., Bartlein, P., Marlon, J., Anderson, R., Behling, H., Brown, K., Carcaillet, C., Colombaroli, D., Gavin, D., Hallett, D., Horn, S., Kennedy, L., Lane, C., Long, C., Moreno, P., Paitre, C., Robinson, G., Taylor, Z., and Walsh, M.: Climatic control of the biomass-burning decline in the Americas after ad 1500, The Holocene, 23, 3–13, 10.1177/0959683612450196, 2013.

Qi, L. and Wang, S.: Sources of black carbon in the atmosphere and in snow in the Arctic, Sci. Total Environ., 691, 442–454, https://doi.org/10.1016/j.scitotenv.2019.07.073, 2019.

Rantanen, M., Karpechko, A. Y., Lipponen, A., Nordling, K., Hyvärinen, O., Ruosteenoja, K., Vihma, T., and Laaksonen, A.: The Arctic has warmed nearly four times faster than the globe since 1979, Comm. Earth Environ., 3, 168, 10.1038/s43247-022-00498-3, 2022.

Rasmussen, S. O., Seierstad, I. K., Andersen, K. K., Bigler, M., Dahl-Jensen, D., and Johnsen, S. J.: Synchronization of the NGRIP, GRIP, and GISP2 ice cores across MIS 2 and palaeoclimatic implications, Quaternary Sci. Rev., 27, 18–28, http://dx.doi.org/10.1016/j.quascirev.2007.01.016, 2008.

Rubino, M., D'Onofrio, A., Seki, O., and Bendle, J. A.: Ice-core recodes of biomass burning, The Anthropocene Rev., 3, 140-162, https://journals.sagepub.com/doi/abs/10.1177/2053019615605117, 2016.

Ruppel, M. M., Isaksson, I., Ström, J., Beaudon, E., Svensson, J., Pedersen,C. A., and Korhola, A.: Increase in elemental carbon values between 1970 and 2004 observed in a 300-year ice core from Holtedahlfonna (Svalbard), Atmos. Chem. Phys., 14, 11447–11460, 10.5194/acp-14-11447-2014, 2014.

Savarino, J. and Legrand, M.: High northern latitude forest fires and vegetation emissions over the last millennium inferred from the chemistry of a central Greenland ice core, J. Geophys. Res.-Atmos., 103, 8267–8279, 10.1029/97jd03748, 1998.

Schmeisser, L., Backman, J., Ogren, J. A., Andrews, E., Asmi, E., Starkweather, S., Uttal, T., Fiebig, M., Sharma, S., Eleftheriadis, K., Vratolis, S., Bergin, M., Tunved, P., and Jefferson, A.: Seasonality of aerosol optical properties in the Arctic, Atmos. Chem. Phys., 18, 11599–11622, 10.5194/acp-18-11599-2018, 2018.

Schwarz, J. P., Gao, R. S., Perring, A. E., Spackman, J. R., and Fahey, D. W.: Black carbon aerosol size in snow, Sci. Rep., 3, 1356, 10.1038/srep01356, 2013.

Sharma, S., Andrews, E., Barrie, L. A., Ogren, J. A., and Lavoué, D.: Variations and sources of the equivalent black carbon in the high Arctic revealed by long-term observations at Alert and Barrow: 1989–2003, J. Geophys. Res.-Atmos., 111, https://doi.org/10.1029/2005JD006581, 2006.

https://doi.org/10.5194/egusphere-2024-1498
Preprint. Discussion started: 23 May 2024

754 Sharma, S., Barrie, L. A., Magnusson, E., Brattström, G., Leaitch, W. R., Steffen, A., and Landsberger, S.: A factor and trends
755 analysis of multidecadal lower tropospheric observations of Arctic aerosol composition, black carbon, ozone, and mercury
756 at Alert, Canada, J. Geophys. Res.-Atmos., 124, 14133–14161, https://doi.org/10.1029/2019JD030844, 2019.
757 Sharma, S., Ishizawa, M., Chan, D., Lavoué, D., Andrews, E., Eleftheriadis, K., and Maksyutov, S.: 16-year simulation of
758 Arctic black carbon: Transport, source contribution, and sensitivity analysis on deposition, J. Geophys. Res.-Atmos., 118,
759 943–964, https://doi.org/10.1029/2012JD017774, 2013.
760 Shindell, D. and Faluvegi, G.: Climate response to regional radiative forcing during the twentieth century, Nat. Geosci., 2,
761 294–300, 10.1038/ngeo473, 2009.
762 Sigl, M., McConnell, J. R., Layman, L., Maselli, O., McGwire, K., Pasteris, D., Dahl-Jensen, D., Steffensen, J. P., Vinther, B.,
763 Edwards, R., Mulvaney, R., and Kipfstuhl, S.: A new bipolar ice core record of volcanism from WAIS Divide and NEEM
764 and implications for climate forcing of the last 2000 years, J. Geophys. Res.-Atmos., 118, 1151–1169,
765 10.1029/2012jd018603, 2013.
766 Sinnl, G., Winstrup, M., Erhardt, T., Cook, E., Jensen, C. M., Svensson, A., Vinther, B. M., Muscheler, R., and Rasmussen, S.
767 O.: A multi-ice-core, annual-layer-counted Greenland ice-core chronology for the last 3800 years: GICC21, Clim. Past, 18,
768 1125–1150, 10.5194/cp-18-1125-2022, 2022.
769 Skakun, R. Whitman, E., Little, J. M., and Parisien, M.-A.: Area burned adjustments to historical wildfires in Canada, Environ.
770 Res. Lett. 16 064014, 2021.
771 Stein, A. F., Draxler, R. R., Rolph, G. D., Stunder, B. J. B., Cohen, M. D., and Ngan, F.: NOAA's HYSPLIT atmospheric
772 transport and dispersion modeling system, B. Am. Meteorol. Soc., 96, 2059–2077, https://doi.org/10.1175/BAMS-D-14-
773 00110.1, 2015.
774 Stephens, M., Turner, N., and Sandberg, J.: Particle identification by laser-induced incandescence in a solid-state laser cavity,
775 Appl. Opt., 42, 3726–3736, 10.1364/AO.42.003726, 2003.
776 van Marle, M. J. E., Kloster, S., Magi, B. I., Marlon, J. R., Daniau, A. L., Field, R. D., Arneth, A., Forrest, M., Hantson, S.,
777 Kehrwald, N. M., Knorr, W., Lasslop, G., Li, F., Mangeon, S., Yue, C., Kaiser, J. W., and van der Werf, G. R.: Historic
778 global biomass burning emissions for CMIP6 (BB4CMIP) based on merging satellite observations with proxies and fire
779 models (1750–2015), Geosci. Model Dev., 10, 3329–3357, 10.5194/gmd-10-3329-2017, 2017.

https://doi.org/10.5194/egusphere-2024-1498
Preprint. Discussion started: 23 May 2024

780 Vinther, B. M., Buchardt, S. L., Clausen, H. B., Dahl-Jensen, D., Johnsen, S. J., Fisher, D. A., Koerner, R. M., Raynaud, D.,
781 Lipenkov, V., Andersen, K. K., Blunier, T., Rasmussen, S. O., Steffensen, J. P., and Svensson, A. M.: Holocene thinning of
782 the Greenland ice sheet, Nature, 461, 385–388, 10.1038/nature08355, 2009.
783 Wang, M., Xu, B., Kaspari, S. D., Gleixner, G., Schwab, V. F., Zhao, H., Wang, H., and Yao, P.: Century-long record of black
784 carbon in an ice core from the Eastern Pamirs: Estimated contributions from biomass burning, Atmos. Environ., 115, 79–
785 88, https://doi.org/10.1016/j.atmosenv.2015.05.034, 2015.
786 Wang, D., Guan, D., Zhu, S., Kinnon, M. M., Geng, G., Zhang, Q., Zheng, H., Lei, T., Shao, S., Gong, P., and Davis, S. J.:
787 Economic footprint of California wildfires in 2018, Nat. Sustain., 4, 252–260, 10.1038/s41893-020-00646-7, 2021.
788 Warren, S. G.: Light-Absorbing Impurities in Snow: A Personal and Historical Account, Front. Earth Sci. 6:250. doi:
789 10.3389/feart.2018.00250, 2019.
790 Wendl, I. A., Menking, J. A., Färber, R., Gysel, M., Kaspari, S. D., Laborde, M. J. G., and Schwikowski, M.: Optimized
791 method for black carbon analysis in ice and snow using the Single Particle Soot Photometer, Atmos. Meas. Tech., 7, 2667–
792 2681, 10.5194/amt-7-2667-2014, 2014.
793 Whitlow, S., Mayewski, P., Dibb, J., Holdsworth, G., and Twickler, M.: An ice-core-based record of biomass burning in the
794 Arctic and Subarctic, 1750–1980, Tellus B, 46, 234–242, https://doi.org/10.1034/j.1600-0889.1994.t01-2-00006.x, 1994.
795 Whitman, E., Parisien, M.-A., Thompson, D. K., Hall, R. J., Skakun, R. S., and Flannigan, M. D.: Variability and drivers of
796 burn severity in the northwestern Canadian boreal forest, Ecosphere, 9, e02128, https://doi.org/10.1002/ecs2.2128, 2018.
797 Wiscombe, W. J. and Warren, S. G.: A model for the spectral albedo of snow. I: Pure snow, J. Atmos. Sci., 37, 2712–2733,
798 doi:10.1175/1520-0469(1980)037<2712:AMFTSA>2.0.CO;2, 1980.
799 Zdanowicz, C. M., Proemse, B. C., Edwards, R., Feiteng, W., Hogan, C. M., Kinnard, C., and Fisher, D.: Historical black
800 carbon deposition in the Canadian High Arctic: a 250-year long ice-core record from Devon Island, Atmos. Chem. Phys.,
801 18, 12345–12361, 10.5194/acp-18-12345-2018, 2018.
802 Zennaro, P., Kehrwald, N., McConnell, J. R., Schüpbach, S., Maselli, O. J., Marlon, J., Vallelonga, P., Leuenberger, D.,
803 Zangrando, R., Spolaor, A., Borrotti, M., Barbaro, E., Gambaro, A., and Barbante, C.: Fire in ice: two millennia of boreal
804 forest fire history from the Greenland NEEM ice core, Clim. Past, 10, 1905–1924, 10.5194/cp-10-1905-2014, 2014.
805

https://doi.org/10.5194/egusphere-2024-1498
Preprint. Discussion started: 23 May 2024

806 **Appendices**

807

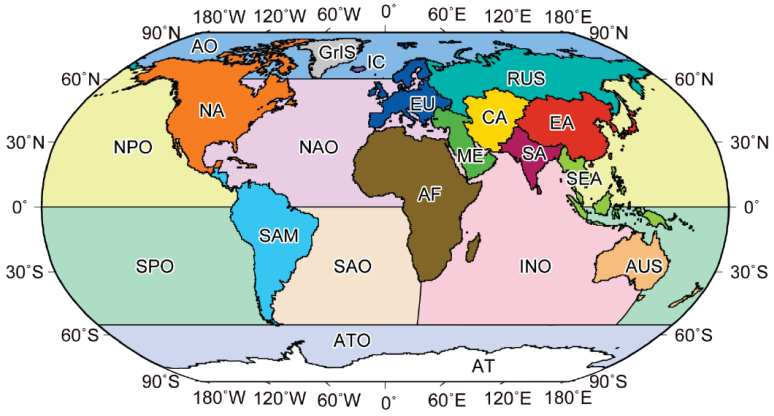

Figure A1: Map showing 21 regions used for calculating the regional contributions in backward trajectory analysis.

ME: Middle East, AT: Antarctica, AUS: Australia and New Zealand, SAM: South America, AF: Africa, EA: China and East Asia, EU: Europe, GrIS: Greenland Ice Sheet, SEA: Southeast Asia, SA: South Asia, CA: Central Asia, RUS: Russia, NA: North America, ATO: Antarctic Ocean, SPO: South Pacific Ocean, INO: Indian Ocean, NPO: North Pacific Ocean, SAO: South Atlantic Ocean, NAO: North Atlantic Ocean, AO: Arctic Ocean, IC: Iceland.

808

809 **Table A1 Biomass burning events distinguished in the SIGMA-D ice core record, and in the records of other ice cores**
810 **and surface snow from Greenland. Records from Greenland sites with temporal resolution of greater than 1 year were**
811 **not used. Events distinguished in the SIGMA-D core were defined using BC mass concentration peaks and NH_4^+**
812 **concentration peaks. For BC, peaks exceeding the summer (May–July) averages + 2σ or 3σ were selected; for NH_4^+,**
813 **peaks exceeding the annual average + 2σ or 3σ were selected. If a BC peak was found in April, August, or September,**
814 **the year is written in parentheses. If a BC or NH_4^+ summer peak in the SIGMA-D core with a concentration between**
815 **the average + 1σ and 2σ was found in the same year when a large biomass burning event was recorded at other**
816 **Greenland sites, the peak was also selected as a biomass burning event. If a year with a biomass burning event reported**

https://doi.org/10.5194/egusphere-2024-1498
Preprint. Discussion started: 23 May 2024

in previous studies agreed with that in the SIGMA-D core within 2 years, the records were considered to reflect the same event, and are written on the same line in the table.

A: Year of the event in the SIGMA-D core

B: Magnitude of the BC mass concentration peak

C: Magnitude of the NH_4^+ concentration peak

D: Year of the event in ice cores and surface snow from Greenland sites other than the SIGMA-D site

E: Location of the ice core or surface snow in Greenland

F: Biomass burning proxies

G: References

SIGMA-D core (This study)			Ice cores and surface snow from Greenland sites other than the SIGMA-D site			
A	B	C	D	E	F	G
Year	Magnitude of BC peak	Magnitude of NH_4^+ peak	Year	Location of ice core or surface snow	Proxy	Reference
1655	>average + 3σ	>average + 2σ	1654 1655	SUMMIT, NEEM SUMMIT	NH_4^+ NH_4^+, $HCOO^-$	(Legrand et al., 2016) (Savarino and Legrand, 1998)
1661	No data	>average + 2σ				
1665	>average + 3σ	>average + 2σ				
1667	>average + 2σ	>average + 1σ				
1675		>average + 3σ				
1684	>average + 1σ		1683	NEEM	NH_4^+	(Legrand et al., 2016)
1690		>average + 3σ				
1692	>average + 2σ					
1697	>average + 3σ	>average + 3σ	1699	SUMMIT	NH_4^+	(Legrand et al., 2016)
			1702–03	NEEM	NH_4^+	(Legrand et al., 2016)

https://doi.org/10.5194/egusphere-2024-1498
Preprint. Discussion started: 23 May 2024

			1702 1703	NEEM NEEM	BC BC	(Zennaro et al., 2014) (Zennaro et al., 2014)
1710	>average + 3σ	>average + 3σ				
1711	>average + 3σ	>average + 1σ				
1712	>average + 3σ	>average + 3σ				
1715	>average + 1σ	>average + 3σ				
1717	>average + 1σ	>average + 2σ	1719	NEEM	NH_4^+	(Legrand et al., 2016)
1724		>average + 2σ				
1727		>average + 3σ	1728	SUMMIT	NH_4^+	(Legrand et al., 2016)
1729	>average + 2σ					
1733	>average + 3σ		1732	NEEM	NH_4^+	(Legrand et al., 2016)
1735	>average + 2σ					
1740		>average + 3σ				
1743	>average + 1σ	>average + 2σ				
1750		>average + 3σ				
1756		>average + 3σ				
1761	>average + 1σ	>average + 3σ				
1765	>average + 2σ	>average + 2σ				
1773	>average + 1σ (>average + 3σ in September)	>average + 3σ	1771 1773 1773	NEEM SUMMIT SUMMIT	NH_4^+ NH_4^+ NH_4^+, $HCOO^-$	(Legrand et al., 2016) (Legrand et al., 2016) (Savarino and Legrand, 1998)
1775	>average + 1σ	>average + 2σ				
1788	>average + 3σ	>average + 3σ				
1789	>average + 2σ (>average + 3σ in August)	>average + 3σ	1789	NEEM	BC	(Zennaro et al., 2014)

https://doi.org/10.5194/egusphere-2024-1498
Preprint. Discussion started: 23 May 2024

1793	>average + 3σ	>average + 3σ	1792	NEEM	NH_4^+	(Legrand et al., 2016)
1794	>average + 1σ	>average + 2σ	1794–95 1795 1795	SUMMIT SUMMIT D4	NH_4^+ NH_4^+, $HCOO^-$ NH_4^+	(Legrand et al., 2016) (Legrand and De Angelis, 1996) (Legrand et al., 2016)
1804	>average + 2σ	>average + 1σ				
1807		>average + 1σ	1807	SUMMIT, NEEM, D4	NH_4^+	(Legrand et al., 2016) (Legrand et al., 2016)
(1812)	(>average + 3σ in April)					
1824	>average + 3σ	>average + 2σ				
1827		>average + 2σ				
1835	>average + 1σ	>average + 3σ	1837	SUMMIT, NEEM, D4	NH_4^+ NH_4^+	(Legrand et al., 2016) (Legrand et al., 2016)
1840	>average + 1σ	No data	1839	SUMMIT SUMMIT	NH_4^+ NH_4^+, HCOO	(Legrand et al., 2016) (Legrand and De Angelis, 1996)
1849	>average + 1σ	No data	1846 1847 1848	SUMMIT D4 NEEM	NH_4^+ NH_4^+ NH_4^+	(Legrand et al., 2016) (Legrand et al., 2016) (Legrand et al., 2016)
1851	>average + 3σ	No data	1853	NEEM	NH_4^+	(Legrand et al., 2016)
		No data	1854	SUMMIT, D4	NH_4^+	(Legrand et al., 2016)
1859	>average + 3σ					
1861	>average + 2σ	>average + 1σ				
1863	>average + 3σ	No data	1863	SUMMIT, NEEM, D4 SUMMIT	NH_4^+ NH_4^+ NH_4^+, $HCOO^-$	(Legrand et al., 2016) (Legrand et al., 2016)

https://doi.org/10.5194/egusphere-2024-1498
Preprint. Discussion started: 23 May 2024

						(Savarino and Legrand, 1998)
		No data	1868 1869	SUMMIT D4	NH_4^+ NH_4^+	(Keegan et al., 2014) (Legrand et al., 2016)
	No data	No data	1871 1872, D4	SUMMIT NEEM	NH_4^+ NH_4^+	(Legrand et al., 2016) (Legrand et al., 2016)
1883	>average + 2σ	No data				
		No data	1886 1888	SUMMIT, NEEM, D4 20D (Dye-3), GISP2 (SUMMIT) NEEM	NH_4^+ NH_4^+ NH_4^+ NH_4^+	(Legrand et al., 2016) (Legrand et al., 2016) (Whitlow et al., 1994) (Legrand et al., 2016)
		No data	1889 1890	SUMMIT D4 SUMMIT	BC, NH_4^+ NH_4^+ NH_4^+	(Keegan et al., 2014) (Legrand et al., 2016) (Legrand et al., 2016)
1894	>average + 1σ (>average + 3σ in April)	No data	1894–95 1894–95 1895	SUMMIT, NEEM, D4 SUMMIT	NH_4^+ NH_4^+ NH_4^+, $HCOO^-$	(Legrand et al., 2016) (Legrand et al., 2016) (Legrand and De Angelis, 1996)
1896	>average + 1σ	No data	1896	SUMMIT	NH_4^+, $HCOO^-$	(Savarino and Legrand, 1998)
1902	>average + 2σ	No data				
1909	>average + 1σ	No data	1908	SUMMIT, D4 SUMMIT SUMMIT	NH_4^+ NH_4^+, $HCOO^-$ BC, NH_4^+	(Legrand et al., 2016) (Savarino and Legrand, 1998) (Keegan et al., 2014)

https://doi.org/10.5194/egusphere-2024-1498
Preprint. Discussion started: 23 May 2024

		No data	1921	NEEM	NH_4^+	(Legrand et al., 2016)
1925	>average + 3σ	No data	1923	SUMMIT, D4	NH_4^+	(Legrand et al., 2016)
1927	>average + 1σ	No data	1927–28	NEEM	NH_4^+	(Legrand et al., 2016)
(1929)	(>average + 3σ in August & September)		1929	SUMMIT, D4	NH_4^+	(Legrand et al., 2016)
1936	>average + 1σ	No data	1936–38	SUMMIT	NH_4^+	(Legrand et al., 2016)
			1938	SUMMIT, NEEM, D4	NH_4^+	(Legrand et al., 2016)
1940	>average + 1σ	No data				
1944	>average + 3σ	No data	1942	NEEM, D4	NH_4^+	(Legrand et al., 2016)
		No data	1950	SUMMIT, NEEM, D4	NH_4^+	(Legrand et al., 2016)
				SUMMIT	NH_4^+, $HCOO^-$	(Savarino and Legrand, 1998)
		No data	1961	SUMMIT, NEEM, D4	NH_4^+	(Legrand et al., 2016)
				SUMMIT	NH_4^+, $HCOO^-$	(Savarino and Legrand, 1998)
				SE-Dome	Levoglucosan	(Parvin et al., 2019)
		No data	1964	SE-Dome	Levoglucosan	(Parvin et al., 2019)
		No data	1972	NEEM	BC	(Zennaro et al., 2014)
			1973	NEEM	NH_4^+	(Legrand et al., 2016)
			1980	SUMMIT, NEEM, D4	NH_4^+	
1994	>average + 2σ	No data	1994	SE-Dome	Levoglucosan	(Parvin et al., 2019)
				SUMMIT	Levoglucosan, NH_4^+,	(Kehrwald et al., 2012; Dibb et al., 1996)

https://doi.org/10.5194/egusphere-2024-1498
Preprint. Discussion started: 23 May 2024

					$HCOO^-$, CH_3COO^-, $(C_2H_2O_4)^{2-}$	
1995	>average + 2σ	No data				
		No data	1998	SE-Dome	Levoglucosan	(Parvin et al., 2019)
	No CFA data	No data	2012	SUMMIT	BC, NH_4	(Keegan et al., 2014)
	No CFA data	No data	2013	SE-Dome	Levoglucosan	(Parvin et al., 2019)

827

828